Title
Chemical characteristics of air from different source regions during the second Pacific Exploratory Mission in the Tropics (PEM-Tropics B)

Journal
Journal of Geophysical Research Atmospheres, 106(D23)

ISSN
0148-0227

Authors
Maloney, JC
Fuelberg, HE
Avery, MA
et al.

Publication Date
2001-12-16

DOI
10.1029/2001JD900100

JOURNAL OF GEOPHYSICAL RESEARCH, VOL. 106, NO. D23, PAGES 32,609–32,625, DECEMBER 16, 2001

Chemical characteristics of air from different source regions during the second Pacific Exploratory Mission in the Tropics (PEM-Tropics B)

Joseph C. Maloney,[1] Henry E. Fuelberg,[1] Melody A. Avery,[2] James H. Crawford,[2] Donald R. Blake,[3] Brian G. Heikes,[4] Glen W. Sachse,[2] Scott T. Sandholm,[5] Hanwant Singh,[6] and Robert W. Talbot[7]

Abstract. Ten-day backward trajectories are used to determine the origins of air parcels arriving at locations of airborne DC-8 chemical measurements during NASA's second Pacific Exploratory Mission in the Tropics B that was conducted during February–April 1999. Chemical data at sites where the trajectories had a common geographical origin and transport history are grouped together, and statistical measures of chemical characteristics are computed. Temporal changes in potential temperature are used to determine whether trajectories experienced a significant convective influence during the 10-day period. Trajectories describing the aged marine Southern Hemispheric category remain over the South Pacific Ocean during the 10-day period, and their corresponding chemical signature indicates very clean air. The category aged marine air in the Northern Hemisphere is found to be somewhat dirtier. Subdividing its trajectories based on the direction from which the air had traveled is found to be important in explaining the various chemical signatures. Similarly, long-range northern hemispheric trajectories passing over Asia are subdivided depending on whether they had followed a mostly zonal path, had originated near the Indian Ocean, or had originated near Central or South America and subsequently experienced a stratospheric influence. Results show that the chemical signatures of these subcategories are different from each other. The chemical signature of the southern hemispheric long-range transport category apparently exhibits the effects of pollution from Australia, southern Africa, and South America. Parcels originating over Central and northern South America are found to contain the strongest pollution signature of all categories, due to biomass burning and other sources. The convective category exhibits enhanced values of nitrogen species, probably due to emissions from lightning associated with the convection. Values of various species, including peroxides and acids, confirm that parcels were influenced by the removal of soluble gas and particle species due to precipitation. Finally, current results are compared with those from the first PEM-Tropics mission that was conducted in the same region during the southern hemispheric dry season (August–October 1996) when extensive biomass burning occurred. Results show that air samples during PEM-Tropics B are considerably cleaner than those of its dry season counterpart.

1. Introduction

NASA's second Pacific Exploratory Mission in the Tropics (PEM-T-B) was conducted over the tropical Pacific Basin during February through April 1999 to study the impact of human and natural processes on the tropospheric chemistry of the region [*Raper et al.*, this issue]. PEM-T-B was conducted to complement and contrast with the first Pacific Exploratory Mission in the Tropics (PEM-T-A) [*Hoell et al.*, 1999]. While PEM-T-A occurred during the southern tropical dry season (August–October 1996) when there was extensive biomass burning over portions of South America and southern Africa, PEM-T-B was conducted during the southern tropical wet season. Thus different chemical and transport conditions were sampled during the two missions.

Concentrations and lifetimes of chemical species in the atmosphere are affected by three major factors: (1) distance between the point of emission and location of measurement, as well as the winds between those two locations, (2) the mechanism of chemical injection (e.g., injected at low levels and transported aloft, or injected as fresh emissions at high altitudes), and (3) the environment during transport (especially moisture and temperature). For example, the lifetime of ozone (O_3) is ~90 days in the dry middle troposphere, but decreases

[1]Department of Meteorology, Florida State University, Tallahassee, Florida.
[2]NASA Langley Research Center, Hampton, Virginia.
[3]Department of Chemistry, University of California, Irvine, California.
[4]Graduate School of Oceanography, University of Rhode Island, Narragansett, Rhode Island.
[5]Department of Earth and Atmospheric Sciences, Georgia Institute of Technology, Atlanta, Georgia.
[6]NASA Ames Research Center, Moffett Field, California.
[7]Institute for the Study of Earth, Oceans, and Space, University of New Hampshire, Durham, New Hampshire.

Paper number 2001JD900100.
0148-0227/01/2001JD900100$09.00

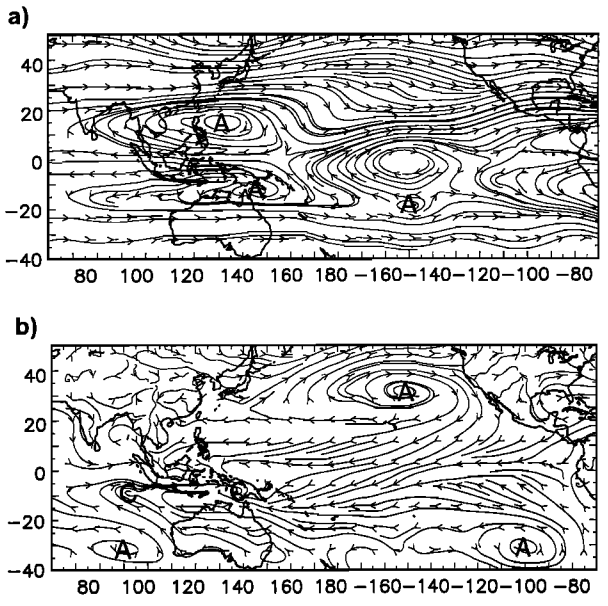

Figure 1. Mean streamlines during the PEM-T-B period (February 25 to April 19, 1999) for (a) 300 and (b) 1000 hPa. Anticyclonic centers are denoted "A," while cyclonic centers are denoted "C" [after *Fuelberg et al.*, this issue, Figure 2].

to 2–5 days in the moist marine boundary layer [*Fishman et al.*, 1991]. Similarly, since peroxyacetyl nitrate (PAN) is stable at cold temperatures, it can be transported long distances in the middle to upper troposphere, but is quickly destroyed in the lower troposphere and marine boundary layer (MBL) [*Singh et al.*, 1990; *Ridley et al.*, 1990]. Thus the altitude at which transport occurs is important to the preservation of some species.

This paper relates the origins of air parcels and their transport histories to their chemical properties during the PEM-T-B period. We examine the 18 DC-8 flights that are described in detail by *Raper et al.* [this issue]. These flights cover an area in the Pacific Basin that ranges from the Solomon Islands eastward to Costa Rica, and from Hawaii to south of Tahiti. Ten-day backward trajectories are calculated to determine origins of the air parcels sampled during these DC-8 flights. Parcels with common origins and similar transport paths are grouped together, and their chemical properties are investigated. Studies that have employed somewhat similar approaches on data sets from previous missions include *Board et al.* [1999], *Gregory et al.* [1996, 1999], and *Talbot et al.* [1994, 1996a, 1996b, 1997].

2. Meteorological Highlights

Chemical species in the atmosphere are transported by the horizontal and vertical winds. *Fuelberg et al.* [this issue] thoroughly discuss the meteorological conditions during PEM-T-B that were important to chemical transport. Thus only the highlights are presented here. The 1000 hPa streamline analysis for the composite PEM-T-B period (Figure 1b) shows two major anticyclones (labeled with "A" letters). One is centered north of Hawaii, and the other is over the South Pacific Ocean near Easter Island (28°S, 109°W). These systems produce the northeasterly and southeasterly trade winds, respectively, that converge near the equator to form the Intertropical Convergence Zone (ITCZ). *Fuelberg et al.* [this issue] note that the ITCZ is not as well defined during the PEM-T-B period as during the northern hemispheric summer and fall period of PEM-T-A. Cyclonic flow near Indonesia (Figure 1b) represents the developing summer monsoon. The South Pacific Convergence Zone (SPCZ) [*Vincent*, 1994] is indicated by convergence aligned northwest-southeast from near New Guinea to Fiji (18°S, 178°E). North of New Guinea the ITCZ and SPCZ merge into a single line of convergence. Both the ITCZ and SPCZ are regions of widespread clouds and precipitation, while the anticyclones generally produce fair skies.

Mean flow patterns at 300 hPa (~9.5 km) (Figure 1a) include a trough axis west of Hawaii, anticyclones just east of the Philippines and in the south-central Pacific Basin, and a clockwise circulation center straddling the equator. Air associated with the northern hemispheric polar jet stream (not shown) travels west-to-east from southern Japan across the northern Pacific, while the subtropical jet stream extends west-southwest to east-northeast from south of Hawaii through Mexico. The southern hemispheric jet stream is located near 30°S, with strongest winds near Australia. The northern hemispheric jets are much stronger than those in the Southern Hemisphere during PEM-T-B.

3. Data and Methodology

3.1. Meteorological Data

The global gridded meteorological data used in this study were prepared by the European Centre for Medium-Range Weather Forecasts (ECMWF) [*ECMWF*, 1995]. The analyses were made at 51 vertical levels with T319 spherical harmonic triangular truncation and were available four times daily (0000, 0600, 1200, and 1800 UTC). The data were transformed to a horizontal grid having a spacing of 1.5° latitude/longitude. The computational domain for most trajectories was 60°S to 75°N and 48°W eastward to 69°W. However, for the final three DC-8 flights, which surveyed the eastern Pacific Basin and the coasts of South and Central America, the western and eastern bounds of the domain were shifted to 0° and 30°W, respectively.

Ten-day backward trajectories were calculated using the Florida State University (FSU) Kinematic Trajectory Model. The kinematic method uses the three dimensional wind components (u, v, and w) to track air parcels without employing the isentropic assumption. Further details about the model, including a comparison between kinematic and isentropic trajectories, are given by *Fuelberg et al.* [1996, 1999, 2000]. Trajectories were checked against a topographic field obtained from the United States Geological Society. Any parcel intersecting either the surface or the 1000 hPa level was terminated at that point.

Trajectories are subject to various limitations, some of which are discussed by *Stohl et al.* [1995], *Stohl* [1998], and *Doty and Perkey* [1993]. The Pacific Basin is a relatively data sparse region. Thus meteorological features may be depicted less accurately than in more data-rich regions. In addition, the horizontal and temporal resolution of the ECMWF data means that small-scale phenomena will not be resolved. For example, individual convective storms (e.g., their updrafts) are not resolved, although the aggregate effects of a convective region are included. Finally, there are numerical limitations in any trajectory model. These factors cause trajectories to become less reliable with increasing time. Nonetheless, the kinematic method has been widely used in previous studies [e.g., *Fuelberg et al.*, 1999; *Hannan et al.*, 2000; *Bieberbach et al.*, 2000; *Stohl and Trickl*, 1999; *Garstang et al.*, 1996].

Arrival locations for the backward trajectories were selected along the 18 DC-8 flight tracks at 5-min intervals of flight time. At an average aircraft speed of 400 kt (206 m s^{-1}), the 5-min interval corresponds to a horizontal separation of ~62 km. To account for potentially mispositioned meteorological features in the ECMWF data, as well as uncertainties due to horizontal and vertical wind shear, a clustering technique was employed [e.g., *Merrill et al.*, 1985; *Kahl*, 1993]. Specifically, a diamond of four additional trajectory points was superimposed on the original 5-min points along the flight track, with each point of the diamond spaced 2° latitude/longitude from the center point. This set of five points also was placed 25 hPa above and 25 hPa below flight level. Thus a cluster of 15 points was created for each original point along the flight track. Trajectories were calculated at 1820 cluster locations along the 18 DC-8 flight tracks during PEM-T-B, giving a total of 27,300 trajectories (1820 × 15). The trajectories arrived at the DC-8 at either 0000, 0600, 1200, or 1800 UTC, whichever was closest to the particular flight time.

3.2. Trajectory Cluster Selection

Trajectory clusters were subjected to three tests to determine whether they could be used with confidence to determine origins of the various chemical samples. The first test considered the effects of horizontal and vertical wind shear. To pass this test, at least ten of the fifteen trajectories in an individual cluster had to exhibit a consistent geographical origin during the preceding ten days. Our five major origin regions are defined later in this section. A cluster was excluded from further consideration if its trajectories did not have a common origin.

The second test checked for major diabatic processes in order to distinguish between two categories of trajectories: convective and nonconvective. To be included in the nonconvective category, at least 10 of the 15 trajectories in a cluster that passed the common origin test could not experience a change of potential temperature (theta) greater than 6°C during any 24 hour period. Conversely, to be included in the convective category, at least 10 of the 15 trajectories must have experienced greater than a 12°C change in theta within a 24-hour period. As a check of this procedure, the trajectories having theta changes greater than 12°C also were required to pass through satellite-observed convection on the day of the large diabatic change. This was determined by visual inspection of the satellite imagery. Other diabatic thresholds were investigated. For example, values smaller than 12°C per day did not exclude many of the trajectories not passing through satellite-observed convection. Conversely, thresholds greater than 12°C reduced the sample size without providing improved agreement with the satellite imagery. Since our goal was to have a clear distinction between convectively influenced trajectory clusters and their nonconvectively influenced counterparts, trajectory clusters with maximum 24-hour theta changes between 6°C and 12°C were excluded from further study.

For the final test, trajectory clusters were examined to ensure that they did not leave the computational domain before 5 days had elapsed. Those clusters that exited the domain between days 5 and 10 remained in the data set only if their geographical origin was obvious at that time.

Our final data set consisted of all trajectory clusters that passed each of the three tests described above. Thus each cluster of the set had at least 10 of 15 trajectories passing both the common origin and theta tests, and remaining within the computational domain for at least 5 days. Of the original 1820 clusters, only 263 passed the three tests, with 166 of them in the nonconvective category and 97 in the convective category. Although this testing procedure greatly reduced our sample size, we believe that the remaining trajectory clusters can be used with confidence to determine the likely origins of air parcels measured by the DC-8. The representativeness of this final data set is discussed in section 3.3.

The 166 clusters that passed the above mentioned tests and did not experience widespread convection were sorted into one of five general categories based on their transport paths and source regions. Horizontal plots and time-height cross sections of trajectories from each of these categories are presented in later sections. Aged Marine Southern Hemisphere (SH) trajectories remained over the Pacific Basin south of the ITCZ during the 10-day period, not passing over any large landmass. We used the ITCZ as the northern boundary since it is a better delineator of northern and southern hemispheric air masses than is the equator [e.g., *Avery et al.*, this issue]. Similarly, Aged Marine Northern Hemisphere (NH) trajectories remained over the Pacific Basin north of the ITCZ during the 10-day period, while not passing over any large land masses. Long-Range NH trajectories originated west of the Pacific Ocean and north of the ITCZ. Many of them traveled over Southeast Asia and/or northern Africa. The Long-Range SH category consisted of trajectories that originated west of the Pacific Ocean and south of the ITCZ. Finally, the South American/Caribbean category contained trajectories that traveled westward from northern South America and the southern Caribbean Sea to the eastern Pacific Basin. Later sections will describe how several of these general categories were subdivided into more specific geographical groups. The second major category, the convectively influenced trajectories, was not divided into geographical categories.

3.3. Chemical Data

We employed a merged chemical data set to link our trajectories to the chemical tracer measurements. This merged data set was prepared at Harvard University from data submitted to the GTE archive by the various DC-8 investigators. These data are available through NASA's GTE web site (http://www-gte.larc.nasa.gov). *Raper et al.* [this issue] discuss the various chemical species measured by the investigators, including the techniques used to make the measurements, the temporal resolution of the measurements, and the level of detection (LOD) for each instrument. The merged data set was a simple 5-min average of the chemical measurements that was centered on the arrival locations (i.e., times) of our trajectories. If a measurement had been flagged in the original data set as being below the LOD, the LOD value was substituted in its place. In the tables of chemical concentrations that follow, LOD values are given in parentheses to identify their contributions to the analyses. As a result of these procedures, each 5-min chemical measurement is associated with a 10-day backward trajectory cluster.

It is important to verify whether our subset of 263 chemical measurements (and corresponding trajectory clusters) is representative of the complete DC-8 data set. Table 1 describes the representativeness of our data set, grouped in four altitude bins. The left column in each bin contains median chemical values for the entire DC-8 data set that were calculated from the complete 5-min merged data set. The right column in each altitude bin shows median values for the trajectory clusters that passed our quality control tests, i.e., selected entries from the

Table 1. Median Concentrations of Chemical Species Observed During PEM-Tropics B[a]

	800–1000 hPa			500–800 hPa		300–500 hPa			<300 hPa	
Species	DC-8		Trj	DC-8	Trj	DC-8		Trj	DC-8	Trj
n	308		48	405	83	515		36	566	96
O_3	14		14	23	24	27	*	17	25	20
CO	53		45	51	48	55		49	50	48
C_2H_6	272		232	275	260	318	*	263	268	254
C_2H_2	17		13	17	17	25	*	14	17	15
PAN	(1)		(1)	14.0	9.2	29.9	*	14.6	18.5	15.9
NO	1.3		1.4	3.7	2.6	9.2		8.6	21.5	25.8
NO_x	5.1		4.9	7.9	6.7	14.7		14.2	30.6	34.7
ΣNO_t	43		54	89	83	87	*	64	93	96
HNO_3	36		49	61	65	41		35	34	34
H_2O_2	772		634	490	548	327	*	233	187	174
CH_3OOH	501	*	442	268	281	184		203	99	77
CH_3I	0.47		0.43	0.12	0.10	0.10		0.13	0.08	0.12
$CHBr_3$	0.86		0.75	0.47	0.39	0.48		0.50	0.45	0.52
^7Be	190		190	306	395	323		394	443	411
C_2Cl_4	1.29		1.16	1.34	1.27	1.54	*	1.29	1.24	1.23

[a]Values in the DC-8 columns represent the complete DC-8 data set, while those in Trj represent values for our final set of 263 trajectory clusters. Mixing ratios are given in parts per trillion by volume (pptv), except for O_3 and CO, which are in parts per billion by volume (ppbv), and ^7Be which is in fCi/scm. LOD values are in parentheses; *n* is the number of trajectory clusters in each altitude interval. An asterisk indicates Trj samples which are significantly different from those of the DC-8 at ≥95% confidence level based on Student's t-test.

5-min merged data set. We examined the statistical representativeness of the trajectory-based samples by performing a standard Student's t-test. An asterisk in Table 1 indicates that the trajectory-based chemical distribution is significantly different from the DC-8 version at the 95% confidence level.

Table 1 indicates that many of our chemical measurements (96 out of 263) were taken in the upper troposphere, with the 500–800 hPa layer being the second most abundant group. Values for some species of our subset between 300 and 500 hPa are somewhat smaller than those of the complete data set, and some are significantly different at the 95% level. This probably is due to the relatively small number of samples that passed the quality controls in this altitude group (36 out of 515). Nonetheless, there generally is good agreement between median values of our subsets and those of the complete DC-8 set. Thus we believe that our subsets generally are representative of the PEM-T-B measurements.

Various atmospheric chemical species can be used to infer the origins of air samples and the influences of convection and mixing. Such inferences generally are not straightforward because parcels may have several origins and species may have been mixed or processed photochemically at various times between emission and sampling. Chemical characteristics of species that we used for this purpose are described below. This section is excerpted from a more detailed discussion in a previous paper by our group [*Board et al.*, 1999].

Ozone (O_3) is an important species for identifying the source of an air mass. Concentrations typically are greatest in stratospherically influenced air (>100 ppbv) and in plumes originating from land sources (70–100 ppbv), but are relatively small in clean air, especially in the tropical MBL (<10 ppbv) [*Gregory et al.*, 1996, 1999; *Talbot et al.*, 1994, 1996a, 1996b, 1997]. Carbon monoxide (CO) also is a reliable indicator of air mass history [*Harriss et al.*, 1992]. Values less than 60 ppbv indicate either stratospherically influenced air or well-aged tropospheric air [*Talbot et al.*, 1996b]. Conversely, tropospheric mixing ratios exceeding 80 ppbv suggest a continental influence. Perchloroethene (C_2Cl_4) is useful for determining whether CO is from biomass burning or urban emissions [*Gregory et al.*, 1996].

In previous studies, the ratio C_2H_2/CO has been used to compare the relative level of atmospheric processing experienced by air parcels of various origins [*Talbot et al.*, 1996a, 1996b, 1997; *Gregory et al.*, 1996, 1999; *Smyth et al.*, 1996; *Board et al.*, 1999]. The utility of this ratio comes from the common combustion source but differing lifetimes of these two species. Some discussions of this ratio have used the term "age." However, changes in the ratio cannot be related directly to time downstream of emissions sources for several reasons. For example, photochemical lifetimes of these species are altitude-dependent. The lifetime of C_2H_2 increases from about 10 days to more than 40 days between the surface and upper troposphere in the low to midlatitudes. Dilutive mixing during transport is an additional influence that can sometimes outweigh photochemistry in changing hydrocarbon ratios [*McKeen and Liu*, 1993; *McKeen et al.*, 1996]. Furthermore, the C_2H_2/CO ratio for the trajectory clusters analyzed here varies proportional to the C_2H_2 mixing ratio. Thus use of the ratio would seem to offer no additional information to the comparisons presented here.

Nitrogen compounds also provide information about air parcel history and the extent of processing. Nitrogen is emitted as NO, which rapidly attains a photochemical steady state with NO_2. Possible sources of NO during PEM-T include lightning [*Ehhalt et al.*, 1992], combustion, and the stratosphere [*Liu et al.*, 1996]. The sum of NO, NO_2, PAN, and nitric acid (HNO_3), hereafter denoted ΣNO_t, typically is enhanced within air influenced by urban processes or biomass burning. PAN and HNO_3 are secondary products of pollution, but HNO_3 also can have a stratospheric origin, and it can be produced by biomass burning [*LeBel et al.*, 1988]. HNO_3 is slowly recycled to NO_2 by photochemistry or is removed rapidly from the atmosphere by particle surfaces or precipitation. Large ratios of NO_x to ΣNO_t, where $NO_x \equiv NO + NO_2$, indicate recent emissions of nitrogen oxides. Large ratios also may indicate recent rapid warming or physical removal of HNO_3.

Chemical tracers of convection, especially marine convection, include methyl iodide (CH_3I), methyl bromoform ($CHBr_3$), "depleted" O_3, and methyl hydroperoxide (CH_3OOH) [*Cohan et al.*, 1999; *Davis et al.*, 1996]. CH_3I and $CHBr_3$ are emitted from seawater, exhibiting large concentrations in the MBL. CH_3I also is produced by biomass burning [*Andreae et al.*, 1996]. The typical lifetime of CH_3I in the tropics is 4 days, while the lifetime of $CHBr_3$ is longer. The lifetime of CH_3OOH is 1–2 days. O_3 is photochemically destroyed in the MBL [e.g., *Kawa and Pearson*, 1989; *Heikes et al.*, 1996b], and its lifetime depends on NO_x, ranging from a week to months [*Liu et al.*, 1987]. Hydrogen peroxide (H_2O_2) also is a tracer of convection [*Heikes*, 1992; *Heikes et al.*, 1996a; *Pickering et al.*, 1996; *Cohan et al.*, 1999]. Both H_2O_2 and CH_3OOH exhibit maxima in the lower troposphere, H_2O_2 near the MBL. H_2O_2 also is a product of biomass burning [*Lee et al.*, 1997]. Once transported aloft, CH_3OOH decays to background values within 1–2 days, whereas H_2O_2 does not decrease significantly during the first several days following convection [*Jaeglé et al.*, 1997; *Cohan et al.*, 1999]. However, H_2O_2 can be removed by precipitation or by reactions in cloud water during transport. The ratio H_2O_2/CH_3OOH <1 has been used to indicate air parcels influenced by recent convection and precipitation [*Heikes*, 1992, 1996a; *Pickering et al.*, 1996; *Cohan et al.*, 1999]. However, its effectiveness as a convective tracer decreases with time due to photochemistry and mixing. Finally, HNO_3 is useful for assessing convective influences. Small values in the upper troposphere may indicate surface layer air which has been depleted of these species by surface removal or by precipitation scavenging [*Talbot et al.*, 1996a].

Beryllium 7 (^7Be) is produced in the upper troposphere and stratosphere by cosmic rays and then absorbed on particles. Beryllium 7 can help identify parcels influenced by convection and particle scavenging processes, and it has been used as a tracer for stratospheric air in the troposphere [*Bhandari et al.*, 1966; *Elbern et al.*, 1997; *Dibb et al.*, 1996, 1997]. Beryllium 7 is depleted from the air by particle removal processes (e.g., sedimentation and precipitation) that occur mostly in the lower troposphere. Large concentrations indicate air that has been in the upper troposphere for a long period of time and has been free of particle removal processes. Beryllium 7 is expected to be depleted in convective outflow of low altitude air that has undergone particle scavenging.

4. Aged Marine—Southern Hemisphere (SH)

A horizontal plot of the sixty 10-day backward trajectory clusters comprising the Aged Marine SH category is shown in Figure 2a. For the sake of clarity, only a single representative trajectory from each cluster is indicated. This trajectory, determined by visual inspection, best describes the origins and paths of all the trajectories comprising that cluster. Thirteen flights of the DC-8 are included in the Aged Marine category. The trajectories remain over the southern Pacific Ocean, south of the ITCZ, during the entire 10-day calculation period. Heights of the representative trajectories are given as a function of time in Figure 2b, with summary statistics presented in Table 2. The chemical measurements (and corresponding trajectory arrival locations) have a median latitude in the deep tropics (15°S). Most trajectories travel toward the west, remaining in the tropics during their 10-day histories. They generally exhibit weak subsidence, with median altitudes at arrival, 5 days back, and 10 days back being, respectively, 771 hPa, 671 hPa, and 570 hPa. Most individual trajectories show only minor altitude variations during the period; however, arrival altitudes (at time equal to 0) range from 391 to 952 hPa (median is 771 hPa). Thus our Aged Marine category not only contains air parcels near the ocean surface, but parcels at any altitude that remain over the ocean during the 10-day trajectory period. Although concentrations of some chemical species are altitude-dependent (e.g., PAN), we have not subdivided this category by altitude, focusing instead on the common horizontal locations of the trajectories.

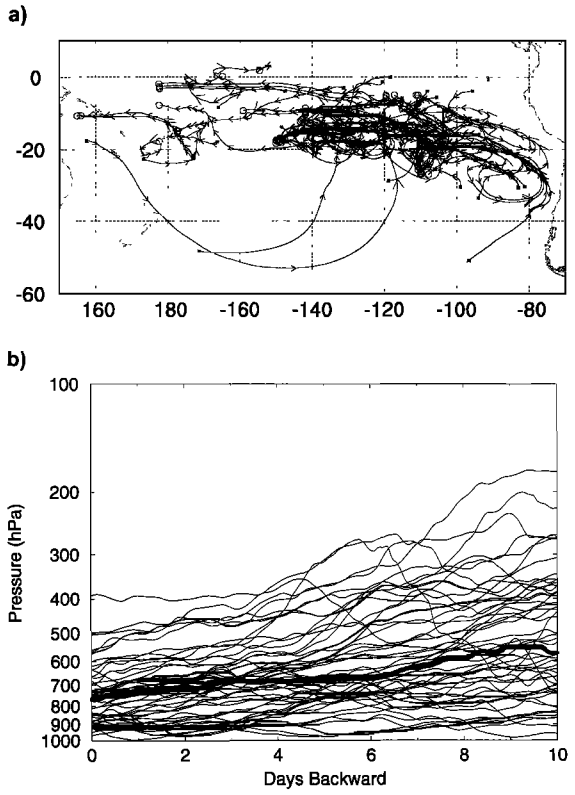

Figure 2. (a) Horizontal plot of 10-day backward trajectories comprising the Aged Marine SH category. For the sake of clarity, only one representative trajectory from each cluster is plotted. Circles indicate trajectory arrival locations along the DC-8 flight tracks, while arrows denote trajectory locations at daily intervals. (b) Time series of altitude for trajectories comprising the Aged Marine SH category. Again, only one representative trajectory from each cluster is plotted. The bold line denotes median altitudes at each time. Trajectories arrive at the DC-8 flight track on day 0.

The chemical measurements in Table 3 confirm the trajectory data, showing that this category consists of relatively clean, well-aged air. For example, median values of species such as O_3 (15 ppbv), CO (46 ppbv), C_2H_2 (13 pptv), PAN (1.6 pptv), and HNO_3 (53 pptv) are among the smallest of our categories. The median ratio of $NO_x/\Sigma NO_i$ is only 0.10, suggesting that the parcels have not received fresh injections of nitrogen species from lightning, jet aircraft, or industrial sources. (Since ΣNO_i requires concurrent measurements of NO, NO_2, PAN, and HNO_3, the number of samples available to compute the ratio (n in the tables) is less than the number for individual nitrogen tracers.)

Values of the first and third quartiles (Table 3) provide information about the distributions of individual chemical spe-

Table 2. Trajectory Data for Air Parcels

	Median Altitude, hPa	Median Latitude, deg N
Nonconvective		
Aged Marine SH		
Arrival	771	−15.0
5 days	671	−15.9
10 days	570	−13.3
Aged Marine NH		
Arrival	775	13.4
5 days	625	12.7
10 days	534	20.9
Long-Range NH		
Arrival	239	16.1
5 days	215	25.7
10 days	210	13.2
Long-Range SH—Low		
Arrival	696	−21.0
5 days	486	−35.5
10 days	381	−37.5
Long-Range SH—High		
Arrival	249	−22.8
5 days	212	−29.2
10 days	178	−30.1
South America—Caribbean		
Arrival	710	9.9
5 days	749	8.4
10 days	724	12.7
Convective		
Arrival	267	−11.6
5 days	750	−10.9
10 days	832	−7.9

cies. One should note that some species exhibit considerable spread even though all the trajectories remain over the South Pacific Ocean during the entire 10-day period. This spread may represent the effects of differing trajectory origins and paths at even earlier times. It would be interesting to determine the sensitivity of the median chemical values to the geographic boundaries of the Aged Marine category. However, that is not feasible since those boundaries are fixed by the locations of the Pacific Ocean and surrounding landmasses.

Table 3. Chemical Characteristics of Principal Species for 60 Aged Marine SH Trajectory Clusters Representing 13 Different Flights[a]

Species	First Quartile	Median	Third Quartile	n
O_3	14	15	23	60
CO	40	46	52	53
C_2H_6	197	245	307	45
C_2H_2	10	13	18	45
PAN	(1)	1.6	6.7	42
NO	1.3	2.6	4.0	37
NO_x	4.9	7.8	10.2	32
ΣNO_t	46	63	91	27
HNO_3	42	53	64	45
$NO_x/\Sigma NO_t$	0.08	0.10	0.18	27
H_2O_2	346	486	802	50
CH_3OOH	129	331	678	50
H_2O_2/CH_3OOH	0.97	1.53	2.91	50
CH_3I	0.10	0.17	0.34	45
$CHBr_3$	0.44	0.64	0.74	45
^7Be	317	417	444	12
C_2Cl_4	1.02	1.18	1.33	45

[a]Mixing ratios for chemicals are given in parts per trillion by volume (pptv), except for O_3 and CO, which are parts per billion by volume (ppbv) and ^7Be which is in fCi/scm. LOD values are in parentheses to indicate their contributions.

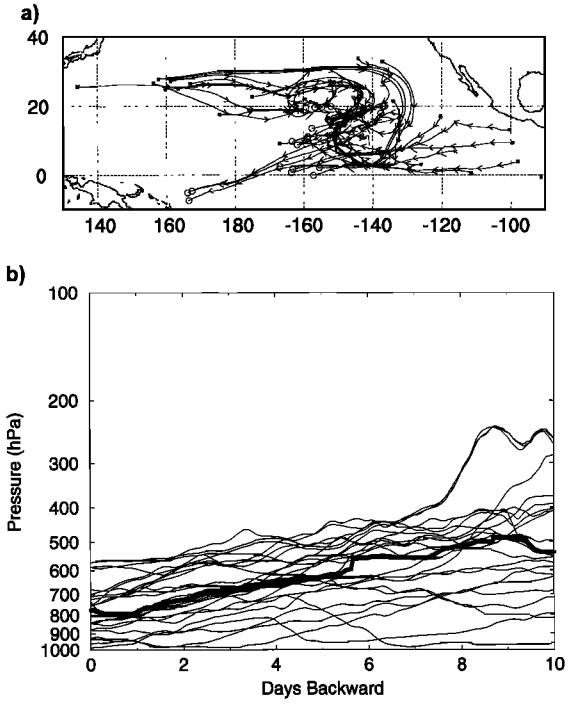

Figure 3. As in Figure 2, but for the Aged Marine NH category.

5. Aged Marine—Northern Hemisphere (NH)

The Aged Marine—NH category consists of 26 trajectory clusters and corresponding chemical measurements from six DC-8 flights (Figure 3a). These trajectories remain over the northern Pacific Basin (north of the ITCZ) during the 10-day period. That is, they do not pass over the adjacent Asian or North American continents during that period. The parcels travel in the lower half of the troposphere (median values are 775, 625, and 534 hPa at arrival, 5 days back, and 10 days back, respectively (Table 2 and Figure 3b)). These median altitudes are similar to those of the Aged Marine SH trajectories.

Chemical measurements for the Aged Marine NH category are shown in Table 4. Most median values are greater than those of the Southern Hemisphere (Table 3), reflecting the greater northern hemispheric landmass, with its associated biogenic and human activity. This difference is evident even though trajectories from both categories are more than 10 days removed from major landmasses. Individual values of most species (not shown) exhibit large ranges, as indicated by the quartile values. Additionally, careful examination of the horizontal plots (Figure 3a) reveals two major transport paths: one from the western Pacific, and the other from the eastern Pacific. On the basis of these two paths we divided the Aged Marine NH category into two subcategories. As a result, the component trajectories had more similar origins and paths, and the corresponding chemical data exhibited a smaller range. A third subcategory consisted of trajectories that were not clearly from the east or from the west, but merely wandered over the Pacific.

Table 4. Chemical Characteristics of Principal Species for 26 Aged Marine NH Trajectory Clusters Representing Six Different Flights[a]

Species	First Quartile	Median	Third Quartile	n
O_3	14	26	42	26
CO	76	81	87	24
C_2H_6	546	597	747	22
C_2H_2	54	73	104	21
PAN	(1)	1.9	21.5	21
NO	1.5	2.0	2.4	21
NO_x	4.8	7.6	13.2	16
ΣNO_t	44	72	106	15
HNO_3	42	73	108	24
$NO_x/\Sigma NO_t$	0.10	0.13	0.15	15
H_2O_2	576	839	1047	24
CH_3OOH	176	547	804	24
H_2O_2/CH_3OOH	1.07	1.78	2.89	24
CH_3I	0.07	0.24	0.41	22
$CHBr_3$	0.37	0.71	0.92	22
^7Be	190	241	453	9
C_2Cl_4	2.59	2.96	3.43	22

[a]Mixing ratios for chemicals are given in parts per trillion by volume (pptv), except for O_3 and CO, which are parts per billion by volume (ppbv) and ^7Be which is in fCi/scm. LOD values are in parentheses to indicate their contributions.

5.1. Aged Marine NH—From the East

Seven of the 26 Aged Marine NH trajectories originate between ~100°–125°W, i.e., well east of their arrival locations along the DC-8 flight tracks (Figure 3a). These trajectories remain in the lower troposphere (mostly below 700 hPa) during the 10-day period (not shown). Thus the parcels are transported to the west by the low-level trade winds. The median chemical values in Table 5 show that the air is cleaner than the Aged Marine NH category as a whole. Some examples include O_3 (11 ppbv from the east versus 26 ppbv for the complete group), C_2H_6 (493 pptv versus 597 pptv), C_2H_2 (41 pptv versus 73 pptv), and HNO_3 (45 pptv versus 73 pptv). On the basis of Student's t-test these differences are all significant at the 95% confidence level. If the trajectories had been extended beyond 10 days, they might have originated over Central America or the northern part of South America. Nonetheless, it appears that parcels arriving at the DC-8 from the east have had sufficient time to be cleansed from any major emissions that they might have received over the Americas. Outflow from Central and South America is discussed in greater detail in Section 8.

Table 5. Comparison of Median Mixing Ratios of Principal Species for the Various Subcategories in the Aged Marine NH Category[a]

Species	West	East	Wandering	Composite
n	12	7	7	26
O_3	43	11	18	26
CO	87	71	78	81
C_2H_6	740	493	597	597
C_2H_2	102	41	65	73
PAN	18.1	(1)	1.4	1.9
NO	2.2	2.3	1.3	2.0
NO_x	18.0	7.0	4.4	7.6
ΣNO_t	115	54	47	72
HNO_3	119	45	44	73
$NO_x/\Sigma NO_t$	0.14	0.15	0.10	0.13
H_2O_2	856	634	892	839
CH_3OOH	547	612	501	547
H_2O_2/CH_3OOH	2.07	0.90	1.68	1.78
CH_3I	0.08	0.15	0.36	0.24
$CHBr_3$	0.37	0.86	1.05	0.71
^7Be	347	320	99	241
C_2Cl_4	2.97	2.46	3.26	2.96

[a]Mixing ratios for chemicals are given in parts per trillion by volume (pptv), except for O_3 and CO, which are parts per billion by volume (ppbv) and ^7Be which is in fCi/scm. LOD values are in parentheses to indicate their contributions.

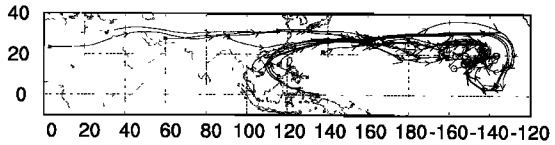

Figure 4. Horizontal plot of 15-day experimental backward trajectories corresponding to the 10-day trajectories of the Aged Marine NH category (Figure 3a) that originate west of the DC-8.

5.2. Aged Marine NH—From the West

Twelve Aged Marine NH trajectories originate west of the flight tracks (Figure 3a), with some extending beyond 160°E at the beginning of the 10-day period. Many of these trajectories follow a curved path, arriving at the DC-8 from the northeast or even southwest. Time-height plots (not shown) indicate that they begin in the mid to upper troposphere during the previous 10 days, subsiding en route to the flight tracks. Thus they first are transported by the upper level westerlies over the central Pacific, then descend in the subtropical Pacific anticyclone (Figure 1b), and finally reverse direction as they are carried by the low-level easterlies to their points of arrival along the flight tracks (Figure 3a). This scenario contrasts with the straight paths and generally lower and more constant altitudes followed by trajectories arriving directly from the east.

Table 5 compares median values of the eastward and westward traveling trajectory groups. There is considerable contrast between values of most species, with parcels coming from the west usually exhibiting the greatest values. Some examples include O_3 (43 ppbv from the west versus 11 ppbv from the east), CO (87 ppbv versus 71 ppbv), C_2H_6 (740 pptv versus 493 pptv), PAN (18.1 pptv versus 1 pptv), and ΣNO_t (115 pptv versus 54 pptv). Each of these differences between the eastward and westward moving groups is significant at the 95% level. Table 5 also shows that the seven trajectories not exhibiting either a clear origin from the east or west (denoted "wandering") generally exhibit chemical signatures that are intermediate to these two categories.

Experimental 15-day back trajectories (Figure 4) were calculated to determine the origins of trajectories arriving from the west. These extended trajectories contain greater uncertainty than the 10-day version shown in Figure 3a. Results indicate that many of the "aged" air parcels originate over Indonesia and skirt the coast of southeast China before heading east. A smaller group of trajectories originates over Asia or northern Africa. Although a few individual 10-day trajectories within some clusters also reached Indonesia, they were not plotted in Figure 3a since they were not the most representative trajectory in the cluster. In addition, their numbers were insufficient to remove them from the Aged Marine NH category.

Southeast China, central Asia, and Indonesia experienced

little biomass burning during the PEM-T-B period [e.g., *Raper et al.*, this issue, Plate 1]. However, these are heavily populated regions with extensive surface-based pollution [e.g., *van Aardenne et al.*, 1999]. There was considerable lightning over Indonesia during the early March period of these trajectories [*Fuelberg et al.*, this issue, Plate 2], but very little lightning in southeastern China and central Asia. The deep convection associated with the lightning may have lofted pollution into the middle troposphere from where it was transported quasi-horizontally to the DC-8. However, this convection apparently was not sufficiently widespread to produce the changes in potential temperature that would have placed the trajectories into the convective category (see section 3.2). In addition, since some trajectories pass over sources of surface pollution at levels near 600 hPa (~4.2 km), cumuliform clouds not tall enough to produce lightning could transport the pollution materials to those altitudes. *Pickering et al.* [1996] provide additional information about the convective transport of chemical species.

In summary, the current data suggest that the "aged marine" trajectories from the west maintain their pollution signature long after departing their emission regions. Thus it is important to know whether aged marine air has traveled from the east or the west, and the length of time since the emissions were injected.

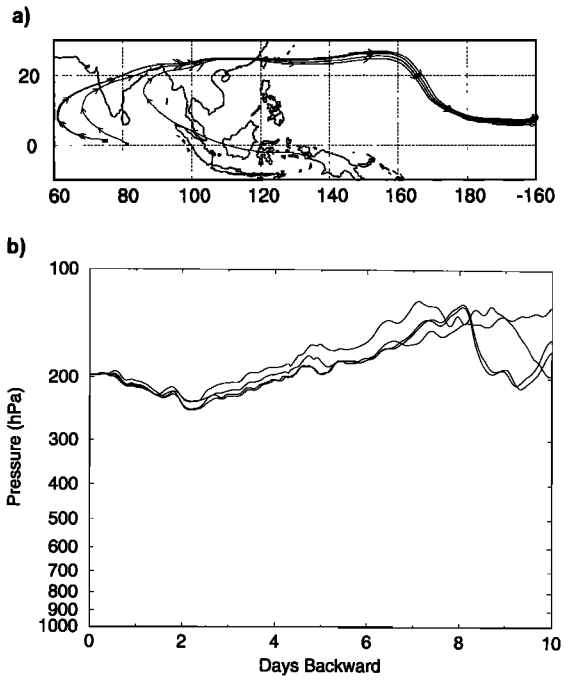

Figure 5. As in Figure 2, but for trajectories in the Long-Range NH category that appear to originate in the Southern Hemisphere.

6. Long-Range NH

The Long-Range NH category consists of 21 trajectory clusters that originate west of the Pacific Basin and north of the ITCZ. Five different DC-8 flights are represented. The category must be subdivided in order to understand the chemical signatures that are observed.

6.1. Southern Hemispheric Influence

Visual inspection suggests that four of the Long-Range NH trajectories experienced a southern hemispheric influence (Figure 5a). These trajectories originate near the equator over the Indian Ocean and Indonesia, i.e., close to the ITCZ and/or SPCZ in the equatorial band of mixing between the two hemispheres [*Avery et al.*, this issue]. The four trajectories show only slight vertical displacements, remaining near 200 hPa throughout the period (Figure 5b).

The chemical signature of the four trajectories is different from that of the long-range category as a whole. Figure 6 is a plot of O_3 versus CO for the 21 trajectories comprising the complete Long-Range NH category. The four points with the smallest CO and O_3 (indicated by diamonds) correspond to the trajectories originating near the equator (Figure 5). Median mixing ratios of O_3 (22 ppbv) and CO (56 ppbv), as well as C_2H_6 (328 pptv) and C_2H_2 (25 pptv), are significantly smaller (95% confidence level) than those of the composite (Tables 6 and 7). On the other hand, the value of NO is significantly greater than that of the composite at the 95% level, while NO_x is only somewhat greater than the composite. These enhancements perhaps are due to lightning and/or biomass burning over portions of India and southeastern Asia. The trajectories may have been influenced by convection associated with the ITCZ and/or SPCZ prior to the 10-day trajectory period. Specifically, HNO_3 (35 pptv) is relatively depleted, while marine tracers such as CH_3I (0.09 pptv) and $CHBr_3$ (0.61 pptv) are somewhat enhanced for air at these altitudes.

It also is informative to compare chemical data of the four trajectories (Table 7) with data for the Marine SH category (Table 3). Values of O_3, CO, hydrocarbons, and nitrogen species for the current trajectories are somewhat greater than those which spent the entire 10-day period away from landmasses in the Southern Hemisphere (Figure 2a). This contrast is consistent with the trajectory data, suggesting that the parcels consist of marine background air that is lofted up by convection in the interhemispheric region and mixed with high-altitude polluted air, perhaps from India and/or southern Asia.

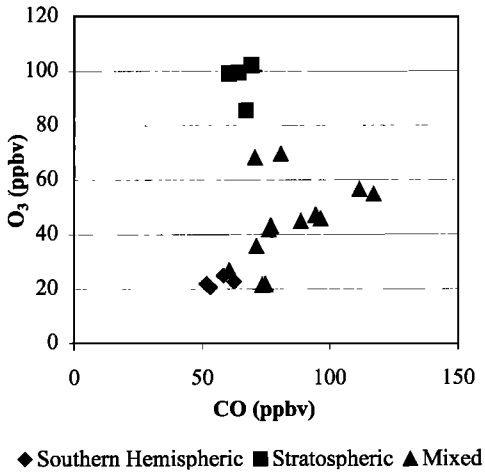

Figure 6. Scatterplot of O_3 versus CO for measurements in the Long-Range NH category. Diamonds indicate trajectories (measurements) that appear to originate in the Southern Hemisphere (Figure 5), squares indicate trajectories with an apparent stratospheric influence (Figure 7), and triangles indicate trajectories with a mixed influence (Figure 8).

Table 6. Chemical Characteristics of Principal Species for 21 Long-Range NH Trajectory Clusters Representing Five Different Flights[a]

Species	First Quartile	Median	Third Quartile	n
O_3	25	45	68	21
CO	62	71	81	21
C_2H_6	438	500	696	19
C_2H_2	41	51	109	19
PAN	22.5	82.9	167.6	19
NO	2.1	4.5	13.4	16
NO_x	20.9	37.7	49.2	11
ΣNO_t	91	228	365	10
HNO_3	42	97	167	21
$NO_x/\Sigma NO_t$	0.12	0.14	0.36	10
H_2O_2	(12)	78	387	18
CH_3OOH	(25)	(25)	227	18
H_2O_2/CH_3OOH	0.48	1.09	2.04	16
CH_3I	0.07	0.09	0.11	19
$CHBr_3$	0.32	0.40	0.58	15
^7Be	368	368	495	5
C_2Cl_4	1.90	2.59	3.05	15

[a]Mixing ratios for chemicals are given in parts per trillion by volume (pptv), except for O_3 and CO, which are parts per billion by volume (ppbv) and ^7Be which is in fCi/scm. LOD values are in parentheses to indicate their contributions.

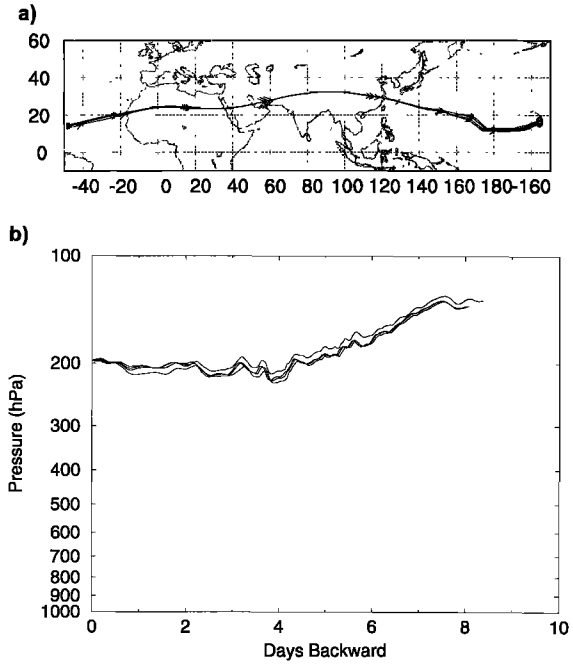

Figure 7. As in Figure 2, but for trajectories in the Long-Range NH category with an apparent stratospheric influence.

6.2. Stratospheric Influence

The four measurements that are marked by squares in Figure 6 exhibit relatively large values of O_3, relatively small values of CO, and are distinct from the other points comprising the complete Long-Range NH category. The four corresponding trajectories originate north of South America near 15°N, and later reach 33°N over central Asia (Figure 7a). The trajectories travel at high altitudes (generally above 200 hPa, Figure 7b), which is comparable to the trajectories with apparent southern hemispheric origins (Figure 5b). However, there is an important difference between the two subcategories. Specifically, the four trajectories associated with greatest O_3 travel farther north, reaching ~33°N compared to ~26°N for those from the Southern Hemisphere. The current trajectories are located near 33°N on March 11, i.e., 4.5 days prior to arriving at the DC-8 (Figure 7a), with altitudes near 200 hPa (Figure 7b). Meteorological charts on that day (not shown) indicate that the tropopause in the area also is near 200 hPa, near the altitude of the jet stream whose winds exceed 60 m s^{-1}. Thus the four trajectories with greatest O_3 are near the altitude of the tropopause across which there is considerable mixing of stratospheric and tropospheric air [e.g., *Danielsen*, 1968; *Reiter et al.*, 1969; *Shapiro*, 1980]. Conversely, meteorological charts show that the southern hemispheric trajectories in Figure 5 remain south of the jet stream and within the troposphere.

Table 7. Comparison of Median Mixing Ratios of Principal Species for the Various Subcategories in the Long-Range NH Category[a]

Species	Southern Hemisphere	Stratosphere	Mixed	Composite
n	4	4	13	21
O_3	22	99	45	45
CO	56	66	77	71
C_2H_6	328	465	657	500
C_2H_2	25	41	89	51
PAN	17.2	177.3	82.9	82.9
NO	31.3	2.0	4.5	4.5
NO_x	43.9	53.6	11.6	37.7
ΣNO_t	97	417	202	228
HNO_3	35	180	97	97
$NO_x/\Sigma NO_t$	0.45	0.13	0.11	0.14
H_2O_2	159	205	70	78
CH_3OOH	99	(25)	244	(25)
H_2O_2/CH_3OOH	2.42	8.20	1.88	1.09
CH_3I	0.09	0.05	0.09	0.09
$CHBr_3$	0.61	...	0.38	0.40
^7Be	...	...	368	368
C_2Cl_4	1.90	...	2.77	2.59

[a]Mixing ratios for chemicals are given in parts per trillion by volume (pptv), except for O_3 and CO, which are parts per billion by volume (ppbv) and ^7Be which is in fCi/scm. LOD values are in parentheses to indicate their contributions.

Median mixing ratios (Table 7) of O_3 (99 ppbv), HNO_3 (180 pptv), and ΣNO_t (417 pptv) are significantly greater (95% level) than those of the composite Long-Range NH category. These enhancements support the stratospheric influence that is suggested by the trajectories. Very small values for marine tracers (e.g., CH_3I, 0.05 pptv) indicate that this air has not been influenced recently by surface air.

The stratospherically influenced parcels may have experienced an additional influence. Specifically, one should note that values of CO, C_2H_6, and C_2H_2 for the stratospherically influenced subcategory (Table 7) are similar to those of the Aged Marine NH-East subcategory (Table 5). In addition, the trajectories in Figures 3a and 7a suggest that parcels in both subcategories may have passed over Central or northern South America 12–15 days earlier. This region contains abundant sources of surface-based pollution. Since the Aged Marine air remained in the humid lower troposphere as it traveled toward the west (Figure 3b), it may have experienced an ozone loss (e.g., median O_3 of 11 ppbv in Table 5). Conversely, deep convection over Central and South America may have lofted some polluted air into the upper troposphere from where it

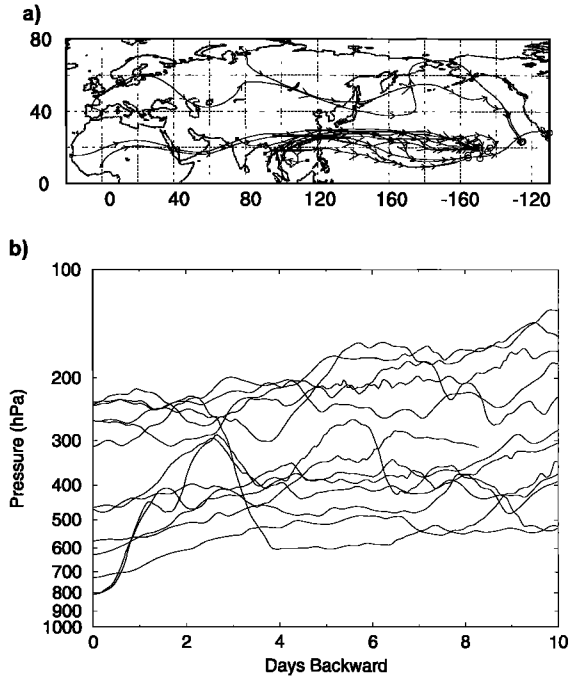

Figure 8. As in Figure 2, but for trajectories in the Long-Range NH category with a mixed influence.

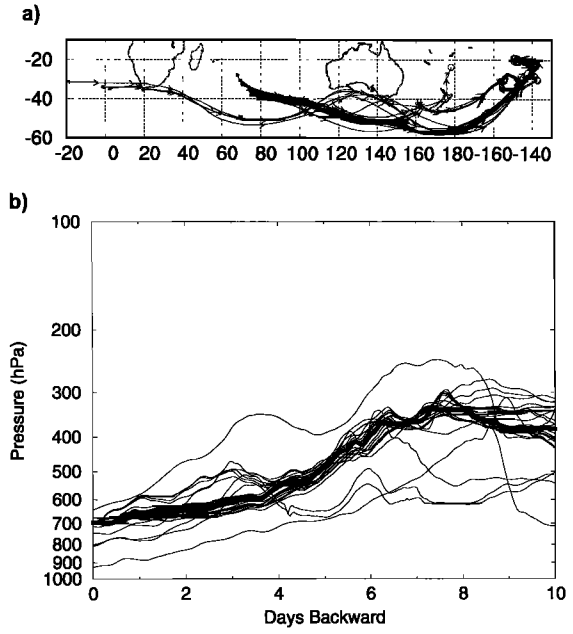

Figure 9. As in Figure 2, but for trajectories in the Long-Range SH—Low altitude arrival category.

was transported eastward. Traveling in the dry upper troposphere, it might have experienced photochemical ozone production (e.g., median O_3 of 99 ppbv in Table 7). Thus the parcels comprising this Long-Range NH subcategory may have been influenced by both long-range pollution sources and more recent stratospheric mixing.

6.3. Mixed Origin

The 13 trajectories that do not have either an obvious southern hemispheric origin or stratospheric influence are plotted in Figure 8. Although these trajectories have a variety of origins, all originate from the west. Most begin near the Bay of Bengal and Southeast Asia, departing the continent approximately 6 days before being sampled by the DC-8. However, two trajectories pass over central Asia, and two others extend over Africa. The trajectories also exhibit a variety of altitudes (Figure 8b), but most are considerably lower than those in the other Long-Range subcategories although some do travel in the upper troposphere.

CO values for this subcategory generally are greater than those of the southern hemispheric and stratospheric subcategories (Figure 6), while O_3 values are intermediate. Table 7 indicates that combustion products such as CO (77 ppbv), C_2H_6 (657 pptv), and C_2H_2 (89 pptv) are enhanced compared to the other subcategories (56 ppbv, 328 pptv, and 25 pptv, respectively, for the southern hemispheric air; and 66 ppbv, 465 pptv, and 41 pptv, respectively, for the stratospherically influenced air). These enhancements are significantly different at the 95% confidence level. The value of C_2Cl_4 (2.77 pptv) suggests that the pollution has an urban origin from Asia.

It is important to note that many of the 10-day trajectory origins and paths in Figure 8a are similar to those of the 15-day trajectories describing the Aged Marine-West subcategory (Figure 4). The major difference is that the current trajectories pass over the coast of Asia ~7 days prior to arriving at the DC-8, while the "aged" trajectories do so ~12 days prior to arrival. Since altitudes of the current trajectories generally are higher (Figures 3b and 8b), the stronger winds at those altitudes produce greater travel distances. The two groups have rather similar chemical characteristics. Some examples are O_3 (45 ppbv current versus 43 ppbv aged from west), CO (77 ppbv versus 87 ppbv), C_2H_6 (657 pptv versus 740 pptv), and NO_x (11.6 pptv versus 18.0 pptv). None of these differences is significant at the 95% confidence level. These chemical similarities suggest that many trajectories in the two groups experience comparable processes in route to the DC-8. However, the trajectories suggest that the parcels experience these processes at different times prior to their sampling by the DC-8.

7. Long-Range SH

Forty-seven trajectory clusters originate south of the ITCZ and west of the Pacific Basin. Trajectories arriving at the DC-8 in the upper troposphere had passed over Australia, while those arriving at the DC-8 in the lower troposphere had traveled south of Australia. On the basis of this distinction we subdivided the Long-Range SH trajectories (and corresponding chemical data) into two groups.

7.1. Long-Range SH—Low-Altitude Arrival

Figure 9a shows the horizontal plot of the 24 trajectories that passed south of Australia on their eastward path to the South Pacific Basin. Most terminate near 70°E at 10 days; however, a few reach as far west as the southern tip of Africa at the beginning of the 10-day period. One should note that these trajectories originate farther south than those of any other category (37.5°S, Table 2) and that many extend as far south as 55°S. Thus, in contrast with our previously discussed categories, the current category contains middle-latitude air. The trajectories arrive in the lower troposphere (median arrival altitude is 696 hPa, Table 2 and Figure 9b), although they originate 10 days earlier in the middle troposphere (381 hPa).

Table 8. Chemical Characteristics of Principal Species for 24 Long-Range SH—Low Arrival Trajectory Clusters Representing Four Different Flights[a]

Species	First Quartile	Median	Third Quartile	*n*
O_3	21	24	26	24
CO	40	42	42	24
C_2H_6	171	175	200	24
C_2H_2	9	10	12	24
PAN	(1)	2.2	9.2	21
NO	0.5	0.8	1.7	20
NO_x	2.6	3.3	4.6	19
ΣNO_t	45	63	76	16
HNO_3	40	55	66	23
$NO_x/\Sigma NO_t$	0.04	0.06	0.09	16
H_2O_2	194	431	610	24
CH_3OOH	126	341	815	24
H_2O_2/CH_3OOH	0.60	1.05	1.84	24
CH_3I	0.08	0.09	0.12	24
$CHBr_3$	0.28	0.30	0.33	24
^7Be	250	250	395	8
C_2Cl_4	0.94	1.01	1.10	24

[a]Mixing ratios for chemicals are given in parts per trillion by volume (pptv), except for O_3 and CO, which are parts per billion by volume (ppbv) and ^7Be which is in fCi/scm. LOD values are in parentheses to indicate their contributions.

Table 9. Chemical Characteristics of Principal Species for 23 Long-Range SH—High Arrival Trajectory Clusters Representing Five Different Flights[a]

Species	First Quartile	Median	Third Quartile	*n*
O_3	31	44	54	23
CO	41	44	46	23
C_2H_6	192	226	251	22
C_2H_2	12	18	20	22
PAN	36.7	51.2	63.2	19
NO	10.6	36.7	40.4	17
NO_x	26.4	44.5	58.3	14
ΣNO_t	148	174	210	12
HNO_3	45	52	108	23
$NO_x/\Sigma NO_t$	0.13	0.17	0.31	12
H_2O_2	47	145	443	22
CH_3OOH	25	154	224	22
H_2O_2/CH_3OOH	0.58	1.41	2.54	22
CH_3I	0.03	0.04	0.06	22
$CHBr_3$	0.19	0.26	0.31	13
^7Be	1024	1024	4454	13
C_2Cl_4	0.66	0.93	1.04	18

[a]Mixing ratios for chemicals are given in parts per trillion by volume (pptv), except for O_3 and CO, which are parts per billion by volume (ppbv) and ^7Be which is in fCi/scm. LOD values are in parentheses to indicate their contributions.

Median values of chemical mixing ratios (Table 8) indicate that the lower tropospheric middle-latitude air is relatively clean, e.g., O_3 (24 ppbv), CO (42 ppbv), C_2H_6 (175 pptv), C_2H_2 (10 pptv), PAN (2.2 pptv), and C_2Cl_4 (1.01 pptv). The trajectory plots indicate that the air is more than 10 days removed from any pollution sources (Figure 9a).

7.2. Long-Range SH—High-Altitude Arrival

Twenty-three trajectory clusters pass over or just south of Australia before reaching the southern Pacific Basin (Figure 10a). Many originate south of Africa, and some even extend to the east coast of South America. These long paths over 10 days are due to the strong winds in the upper troposphere. Like their lower-altitude counterparts discussed above, many of these trajectories extend into the middle latitudes. All 23 arrive at the DC-8 at altitudes above the highest arrival of the Long-Range SH—Low category discussed earlier, remaining in the upper troposphere during their 10-day treks (Table 2 and Figure 10b).

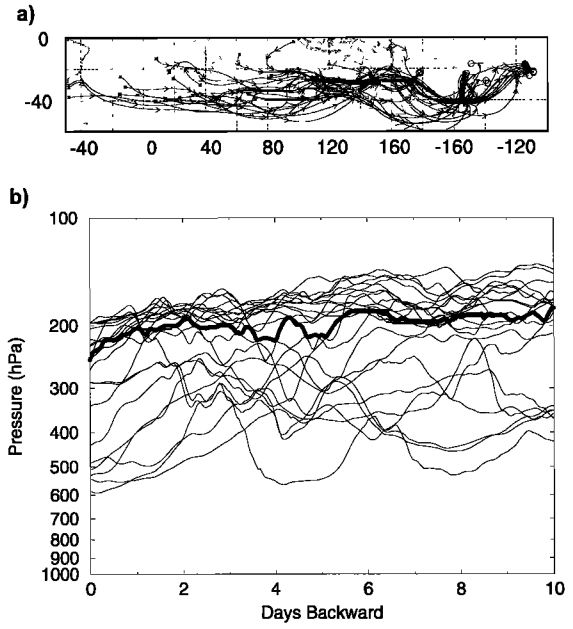

Figure 10. As in Figure 2, but for trajectories in the Long Range SH—High altitude arrival category.

This category exhibits some suggestion of a stratospheric influence (Table 9). Although the median mixing ratio of O_3 is only 44 ppbv, mixing ratios of three individual parcels exceed 95 ppbv (not shown). In addition, these three parcels exhibit ^7Be exceeding 4400 fCi/scm. The median value of ^7Be (1024 fCi/scm) is the largest of any category. Even small amounts of stratospheric air can deliver large amounts of ^7Be to the troposphere [*Board et al.*, 1999]. Another possible mechanism producing large ^7Be is air remaining just below the tropopause for a week or more [*Board et al.*, 1999]. Since the high altitudes of the trajectories suggest that they avoided moist convection, scavenging is inefficient. Furthermore, dry deposition should be small due to the small sizes of the aerosols on which ^7Be is absorbed. Thus the concentration of ^7Be increases.

The upper level category (Table 9) is somewhat more polluted than its lower-level counterpart (Table 8). The CO sample (median of 44 ppbv) (Table 9) is statistically similar (95% confidence level) to that of the Long-Range SH—Low category (median of 42 ppbv) (Table 8). Marine tracers, such as CH_3I (0.04 pptv), $CHBr_3$ (0.26 pptv), H_2O_2 (145 pptv), and CH_3OOH (154 pptv) are small, as expected in air far removed from the ocean surface. However, nitrogen species such as NO (36.7 pptv), NO_x (44.5 pptv), and PAN (51.2 pptv) are significantly greater (95% level) than those of the lower-arriving subcategory (medians of 0.8 pptv, 3.3 pptv, and 2.2 pptv, respectively). These enhancements suggest that the long-range, high-altitude air has been influenced by pollution from Australia, southern Africa, and South America.

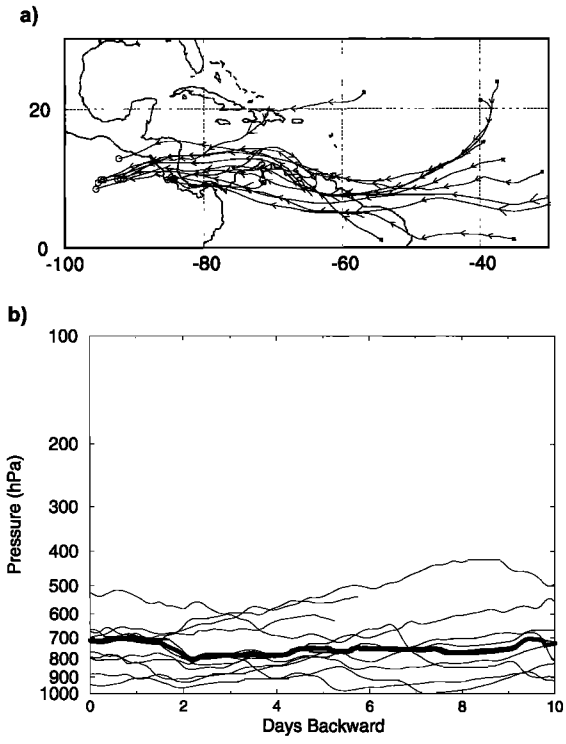

Figure 11. As in Figure 2, but for trajectories in the South American—Caribbean category.

Table 10. Chemical Characteristics of Principal Species for 12 South American—Caribbean Trajectory Clusters Representing Two Different Flights[a]

Species	First Quartile	Median	Third Quartile	n
O_3	23	25	27	12
CO	88	99	108	10
C_2H_6	1254	1573	1683	10
C_2H_2	95	127	195	10
PAN	32.5	84.8	125.8	8
NO	9.7	13.1	13.5	8
NO_x	25.0	26.6	31.7	7
ΣNO_i	253	366	439	6
HNO_3	141	189	237	8
$NO_x/\Sigma NO_i$	0.06	0.08	0.11	6
H_2O_2	1216	1334	1922	10
CH_3OOH	163	294	389	10
H_2O_2/CH_3OOH	4.04	4.54	5.59	10
CH_3I	0.22	0.53	0.67	10
$CHBr_3$	0.56	1.07	2.19	10
^7Be	86	105	123	2
C_2Cl_4	2.19	2.41	2.48	10

[a]Mixing ratios for chemicals are given in parts per trillion by volume (pptv), except for O_3 and CO, which are parts per billion by volume (ppbv) and ^7Be which is in fCi/scm. LOD values are in parentheses to indicate their contributions.

8. South America—Caribbean

Twelve trajectory clusters from two flights passed over northern South America and the southern Caribbean Sea before being sampled by the DC-8 just west of Central America (Figure 11a). Time-height plots (Figure 11b) show that the parcels remain in the lower troposphere during their 10-day histories (Table 2).

Parcels comprising this category exhibit a strong pollution signature (Table 10). Although the median value of O_3 is not large (25 ppbv), carbon species exhibit greatly enhanced mixing ratios, e.g., CO (99 ppbv), C_2H_6 (1573 pptv), C_2H_2 (127 pptv), and C_2Cl_4 (2.41 pptv). Nitrogen species also are enhanced. For example, PAN (84.8 pptv) is quite large for parcels at such low altitudes, and ΣNO_i (366 pptv) is enhanced. The value of HNO_3 (189 pptv) is the largest of our categories, likely due to biomass burning [e.g., *LeBel et al.*, 1988].

The values in Table 10 are consistent with a combustion origin. The trajectories (Figure 11a) indicate that the air passed over northern South America approximately 4–5 days prior to arriving at the DC-8, and over Central America 1–2 days prior to arrival. Northern South America and Central America contain factories, petroleum refineries, and other anthropogenic sources. In addition, there was extensive biomass burning over this region during PEM-T-B [see *Raper et al.*, this issue, Plate 1]. The median mixing ratio for H_2O_2 (1334 pptv) is larger than any other category, including the marine categories, probably due to the biomass burning [e.g., *Lee et al.*, 1997]. There also was extensive lightning over this region [*Fuelberg et al.*, this issue, Plate 2]. Lightning is a known source of nitrogen compounds [e.g., *Lawrence et al.*, 1995].

These results indicate that westward transport from northern South America and Central America was an important mechanism for polluting the eastern Pacific region during PEM-T-B. Conversely, previous sections showed that parcels arriving from the west (easterly transport) did not exhibit a significant pollution signature.

9. Convective Category

The Convective category consists of 97 trajectory clusters from 11 DC-8 flights (Figure 12a). Trajectories in each cluster experienced a large diabatic change (>12°C) during a 24-hour period prior to arriving at the DC-8. In addition, they passed through broad, persistent regions of satellite-observed convection, usually associated with the ITCZ or the SPCZ. Since only a few trajectories travel over land, the category mainly represents marine convection. The daily satellite imagery, altitude versus time plots (Figure 12b), and diabatic changes (not shown) suggest that the parcels are affected by convection an average of 3 days prior to arriving at the DC-8 flight track. However, individual trajectories are convectively processed anywhere from 1–8 days beforehand. The trajectories originate closer to the equator (8.0°S, Table 2) than those of any other category, and they arrive at the DC-8 closer to the equator (11.6°S) than every category except the South America—Caribbean category.

The convectively influenced trajectories originate at low altitudes (median of 832 hPa) but ascend quickly, arriving at a median height of 267 hPa (Table 2 and Figure 12b). This scenario contrasts with the various nonconvective categories (described earlier), whose trajectories exhibit relatively little vertical displacement during the 10-day period. It is important to reemphasize that trajectories based on the ECMWF-derived flow may be very different from trajectories in the true atmosphere, especially in the convective category (Figure 12). At any one time, some parcels may ascend much more rapidly in convective updrafts than indicated by the relatively coarse ECMWF data. Conversely, other parcels may experience convective descent. These variations in altitude also impact the horizontal component of the trajectories due to vertical wind

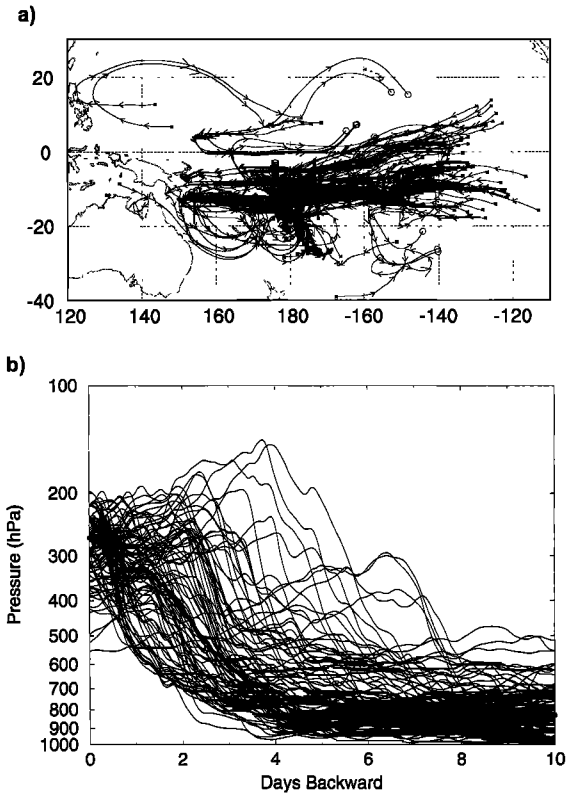

Figure 12. As in Figure 2, but for trajectories in the Convective category.

shear. As a result of these processes, the convective category will contain a wide spectrum of chemical ages since leaving the boundary layer.

Since most of the convectively influenced trajectories remain over the South Pacific Ocean (Figure 12a), it is appropriate to compare their chemical characteristics (Table 11) with those of our Aged Marine SH category (Table 3). Median mixing ratios of O_3 (16 ppbv), CO (48 ppbv), C_2H_6 (247 pptv), and C_2H_2 (14 pptv) for the convection group compare closely to those of the Aged Marine SH trajectories. The differences are not significant at the 95% confidence level. However, the Convective category exhibits greater values of NO and NO_x (15.8 pptv and 22 pptv, respectively) than the Aged Marine SH air (2.6 pptv and 7.8 pptv, respectively), and these differences are significant at the 95% level. The greater NO and NO_x, coupled with an enhanced $NO_x/\Sigma NO_i$ ratio (0.32), suggest recent injections of NO and NO_2, likely from lightning associated with the convection [*Ehhalt et al.*, 1992; *Talbot et al.*, 1996b]. Although lightning over the oceans was less frequent than over land during PEM-T-B, *Fuelberg et al.* [this issue, Plate 2] show that considerable lightning occurred over the tropical Pacific where these trajectories are located.

Table 11. Chemical Characteristics of Principal Species for 97 Convective Trajectory Clusters Representing 11 Different Flights[a]

Species	First Quartile	Median	Third Quartile	*n*
O_3	15	16	20	97
CO	47	48	50	81
C_2H_6	206	247	275	90
C_2H_2	11	14	16	90
PAN	8.3	11.5	16.4	83
NO	8.8	15.8	30.4	78
NO_x	14.4	22.0	36.7	64
ΣNO_i	54	69	95	54
HNO_3	17	30	39	94
$NO_x/\Sigma NO_i$	0.25	0.32	0.43	54
H_2O_2	152	193	306	88
CH_3OOH	52	127	600	88
H_2O_2/CH_3OOH	0.62	1.89	3.26	88
CH_3I	0.11	0.14	0.18	90
$CHBr_3$	0.45	0.53	0.59	90
^7Be	149	259	449	49
C_2Cl_4	1.08	1.25	1.42	90

[a]Mixing ratios for chemicals are given in parts per trillion by volume (pptv), except for O_3 and CO, which are parts per billion by volume (ppbv) and ^7Be which is in fCi/scm. LOD values are in parentheses to indicate their contributions.

We investigated the sensitivity of the medians in Table 11 to varying the convective threshold. For example, when the diabatic change threshold was changed from >12°C to >13°C, the sample size was reduced from 97 clusters to 75. However, values of almost all the species in Table 11 varied by less than 1 ppbv (CO and O_3) or less than 1 pptv (other species). These results indicate that the convective signature is rather insensitive to at least small changes in the diabatic threshold selected.

Various tracers confirm that parcels comprising the Convective category are influenced by the removal of soluble gas and particle species due to precipitation associated with the convection. For example, the median mixing ratio of HNO_3, a soluble tracer, is depleted in the Convective category (30 pptv, Table 11) compared to the Aged Marine category (53 pptv, Table 3). Beryllium 7 (259 fCi/scm) also is much smaller than in the nonconvective southern hemispheric marine air (417 fCi/scm) due to removal by the convection. The median mixing ratio of CH_3I (0.14 pptv) in the Convective category is somewhat smaller than for aged marine air (0.17 pptv). Since CH_3I has a typical lifetime of ~4 days and our trajectories are approximately 3 days removed from convection, it is unlikely that CH_3I has been significantly processed photochemically. Nonetheless, this mixing ratio is greater than the background value measured by the DC-8 above 300 hPa (0.08 pptv, Table 1).

CH_3OOH (127 pptv in the Convective category) is not subject to precipitation scavenging, but does have a short photochemical lifetime (~1–2 days). Thus its depleted value compared to aged marine air (331 pptv) is indicative of rapid decay from photochemical processing. H_2O_2 has a median mixing ratio of 193 pptv, compared to 486 pptv for Aged Marine SH air. Unlike CH_3OOH, H_2O_2 is soluble and subject to scavenging in convection and moist clouds [*Cohan et al.*, 1999]. However, H_2O_2 has a longer lifetime (~3–5 days) than CH_3OOH because the photochemical decay of CH_3OOH cycles to create H_2O_2 [*Cohan et al.*, 1999]. The ratio of the peroxides H_2O_2/CH_3OOH also can identify convectively influenced parcels. For very fresh convection emissions, this ratio is less than one, due to the preferred scavenging of H_2O_2 over CH_3OOH [*O'Sullivan et al.*, 1999]. Background values for this ratio in the upper troposphere typically are greater than 3 [*Heikes et al.*, 1996a; *Lee et al.*, 1998; *Cohan et al.*, 1999; *O'Sullivan et al.*, 1999]. The median value of 1.89 for our convective category is smaller than this background value, indicating somewhat aged convective outflow.

Cohan et al. [1999] used chemical criteria to study "fresh" and "aged" convective outflow compared to background air. The mixing ratios from our trajectory-derived convection cat-

egory generally fall between values of their "aged" convective outflow and background groups. For example, our median mixing ratio of CH_3OOH (127 pptv) compares better with their background mixing ratio (80 pptv) than their aged convective outflow mixing ratio (230 pptv). On the other hand, species such as CH_3I and $CHBr_3$ (0.14 pptv and 0.53 pptv, respectively) compare more favorably with the aged convective outflow (0.15 pptv and 0.44 pptv, respectively) than the background air (0.05 pptv and 0.33 pptv, respectively). This is expected since, as noted above, the trajectory clusters typically experience convection ~3 days prior to arrival. The photochemical lifetimes of CH_3OOH, CH_3I, and $CHBr_3$ are 1–2 days, ~4 days, and >4 days, respectively. Thus much of the convective signal of some species is likely lost in 3 days.

10. Comparisons With PEM-Tropics A

The PEM-T-B mission (February–April 1999) was designed to contrast with conditions during PEM-T-A (August–October 1996). Thus it is informative to compare current results with those from PEM-T-A. As noted earlier, PEM-T-A took place during the southern tropical dry season, while PEM-T-B occurred during the southern tropical wet season.

Most PEM-T-A flights occurred in the southern hemisphere, and *Board et al.* [1999] only examined the southern hemispheric DC-8 flight segments. Therefore their Aged Marine category can be compared to the current Aged Marine SH category. In both cases the Aged Marine trajectories remained south of the ITCZ over the Pacific Ocean. Results show that the Aged Marine SH air during PEM-T-B (Table 3) is much cleaner than its PEM-T-A counterpart [*Board et al.*, 1999, Table 3]. Typical median values are O_3 (15 ppbv during PEM-T-B versus 34 ppbv during PEM-T-A), CO (46 ppbv versus 56 ppbv), and C_2H_2 (13 pptv versus 30 pptv). As noted earlier, there was extensive biomass burning in the Southern Hemisphere during PEM-T-A, but little burning during PEM-T-B. Furthermore, the PEM-T-B aged marine air probably had been separated from distant pollution sources for a longer time than its PEM-T-A counterpart due to the slower speeds of the southern hemispheric jet stream during PEM-T-B [*Fuelberg et al.*, this issue].

Results from the *Board et al.* [1999] Long-Range transport from the west category can be compared with those from the current PEM-T-B Long Range SH—High altitude category. In both cases, trajectories originated in the Southern Hemisphere, west of the tropical Pacific Basin. Although many of the PEM-T-A 10-day trajectories extended as far west as South America and southern Africa [*Board et al.*, 1999, Figure 3b], few PEM-T-B trajectories reached those locations within 10 days (Figure 10a) due to the slower jet level winds. However, many PEM-T-B trajectories probably would reach those locations if the trajectories were extended beyond 10 days.

The Long-Range air during PEM-T-A was impacted by biomass burning emissions from southern Africa and South America. Conversely, there was little biomass burning in the Southern Hemisphere during PEM-T-B. Thus the Long-Range category of PEM-T-A exhibited much larger values of species such as O_3 (82 ppbv during PEM-T-A versus 44 ppbv during PEM-T-B), CO (70 ppbv versus 44 ppbv), PAN (105 pptv versus 51 pptv), and HNO_3 (145 pptv versus 52 pptv) [*Board et al.*, 1999, Table 4] (Table 9). The chemical signature of the South American—Caribbean category during PEM-T-B (Table 10) has many similarities to that of the PEM-T-A Long-Range category. For example, selected South American—Caribbean medians are O_3 (25 ppbv), CO (99 ppbv), PAN (85 pptv), and HNO_3 (189 pptv). The much smaller value of O_3 during PEM-T-B probably is due to the much lower altitudes of these trajectories.

Finally, it is useful to compare chemical signatures of the Convective categories during the two PEM periods [i.e., *Board et al.*, 1999, Table 8] (Table 11). Although each sample contains both northern and southern hemispheric parcels, the convective criteria used in the two studies are somewhat different. Nonetheless, the PEM-T-A convective category is more polluted than its counterpart during PEM-T-B, probably due to the much greater biomass burning in the Southern Hemisphere during PEM-T-A. Some example comparisons of medians are O_3 (33 ppbv for PEM-T-A versus 16 ppbv for PEM-T-B), CO (57 ppbv versus 48 ppbv), and C_2H_2 (37 pptv versus 14 pptv). Examples of nitrogen species are NO (29 pptv PEM-T-A versus 15.8 pptv PEM-T-B) and NO_x (25 pptv versus 22 pptv). Although the PEM-T-B period contained more lightning than the earlier mission [*Fuelberg et al.*, 1999; this issue], the associated greater production of NO and NO_x appears to be overwhelmed by the much greater biomass burning during PEM-T-A. Values of the convective tracers do not exhibit a clear distinction between the two experiments. Some examples are HNO_3 (26 pptv PEM-T-A versus 30 pptv for PEM-T-B), H_2O_2 (244 pptv versus 193 pptv), CH_3OOH (148 pptv versus 127 pptv), and CH_3I (0.08 pptv versus 0.14 pptv).

11. Summary and Conclusions

Chemical data gathered by NASA's DC-8 aircraft have been used with 10-day backward trajectories to investigate atmospheric chemistry over the tropical Pacific Basin during NASA's second Pacific Exploratory Mission in the Tropics (February–April 1999). Backward trajectories were calculated from locations along the 18 DC-8 flight tracks where chemical measurements were taken. Trajectories were subjected to three tests to determine whether they could be used with confidence to determine the origins and paths of parcels. Temporal changes in potential temperature were used to locate trajectories that experienced a significant convective influence during the 10-day period. The trajectories not experiencing significant convection were placed into five major categories based on their origins. The trajectories that did experience significant convection were not subdivided into geographical categories.

Trajectories describing the Aged Marine SH category remained over the open South Pacific waters during the entire 10-day calculation period. The chemical data for this category indicated relatively clean, well-aged air. Median mixing ratios of species such as O_3, CO, C_2H_2, PAN, and HNO_3 were among the smallest of any category.

The Aged Marine air in the Northern Hemisphere category was somewhat "dirtier" than its southern hemispheric counterpart. On the basis of the trajectory data we subdivided this category into three components based on the direction from which the air had traveled. Parcels arriving from the east in the trade winds exhibited a cleaner chemical signature than the composite northern hemispheric aged marine category. Conversely, parcels arriving from the west exhibited enhanced values of O_3, CO, hydrocarbons, and nitrogen species. Their values were greater than those of trajectories arriving from the east. Experimental 15-day back trajectories indicated that

many of the parcels arriving from the west originated over Indonesia and skirted the coast of southeastern China. A smaller group of trajectories originated over central Asia. As the parcels were transported by the upper level westerlies to the central Pacific, they descended in the subtropical Pacific anticyclone, and then were carried by the low-level easterlies to their points of arrival along the DC-8 flight tracks.

Southeastern China, central Asia, and Indonesia are heavily populated, containing extensive sources of surface-based pollution. Deep convection over Indonesia may have lofted these pollutants into the middle troposphere from where they were transported to the DC-8. In addition, since some trajectories passed over sources of surface pollution at levels near 600 hPa (~4.2 km), cumuliform clouds not even tall enough to produce lightning could transport the pollution materials upward to those altitudes. The trajectories that did not originate clearly from the east or west generally exhibited chemical signatures that were intermediate to these two categories. These results show that a simple "aged marine" designation was insufficient to explain the chemical signatures that were observed; more detailed categories that considered the direction of transport were needed.

The Long-Range NH category contained trajectories which had traveled long distances from the west during the 10-day period. This broad category also had to be subdivided in order to understand the observed chemical signatures. One subcategory contained trajectories that originated in the equatorial band of mixing between the two hemispheres. Their chemical data exhibited small values of CO and O_3; however, values of NO and NO_x were greater than those of the composite category, perhaps due to scattered lightning or biomass burning. Values of most species were greater than those of the Aged Marine SH category which remained over the South Pacific for at least 10 days. These results suggest that air in the interhemispheric mixing zone was lofted upward by convection and then mixed with high-altitude polluted air, perhaps from India and/or southern Asia.

Chemical measurements at some of the Long-Range NH trajectory locations exhibited a stratospheric influence as well as influence from surface-based pollution. For example, the median mixing ratio of O_3 was 99 ppbv, the largest of any of our categories. The corresponding trajectories traveled near the altitude of the tropopause in the vicinity of a strong jet stream where there is considerable mixing of tropospheric and stratospheric air. These parcels may have passed over Central America or northern South America ~12 days prior to sampling by the DC-8. Thus their enhanced values of CO, C_2H_6, and C_2H_2 may reflect the widespread surface-based pollution in that area.

The remaining trajectories of the Long-Range NH category originated from a variety of locations, but mostly near the Bay of Bengal and Southeast Asia. Their origins and paths were similar to those of the Aged Marine NH subcategory that arrived from the west; however, the Long-Range trajectories generally traveled at higher altitudes. Thus trajectories of the Long-Range category required ~7 days to reach the coast of Asia, while the Aged Marine NH group required ~12 days. Chemical characteristics of these two groups also were similar, suggesting that both experienced similar processes en route to the DC-8. The dominant mechanism appears to be convective transport of surface based pollution followed by long-range transport.

Many trajectories traveled long distances in the southern hemispheric westerlies. Those arriving at the DC-8 in the lower troposphere had passed south of Australia in the middle latitudes, mostly originating over the central Indian Ocean. This air exhibited a relatively clean chemical signature. A second long-range southern hemispheric category contained trajectories that passed over or near Australia, arriving at the DC-8 in the upper troposphere. Many of these trajectories extended back to the South Atlantic Ocean during the 10-day period. Their chemical signature was somewhat dirtier than the lower-level counterpart, probably due to pollution from distant sources such as South America and southern Africa. In addition, some stratospheric influence was suggested by large values of ^7Be (>4400 fCi/scm) that corresponded to large values of O_3 (>95 ppbv).

The DC-8 sampled air that had passed over Central America and the northern portion of South America. Parcels in this category exhibited a strong pollution signature, with greatly enhanced values of carbon and nitrogen species. These areas contain various industrial sources of pollution, and there was extensive biomass burning and lightning in the area. The trajectory data indicated that the air was 1–5 days removed from its emission sources. These results suggest that transport from Central America and northern South America was an important mechanism for polluting the eastern Pacific.

Our final category consisted of trajectories which experienced a large change in potential temperature. This large diabatic effect corresponded to the time and location of satellite-observed deep convection, mostly near the ITCZ or SPCZ and away from large landmasses. The parcels were influenced by this convection an average of 3 days prior to arriving at the DC-8. The trajectories originated in the lower troposphere, but ascended quickly while influenced by the convection, arriving at the DC-8 in the upper troposphere. Values of carbon species in the convectively influenced category generally were similar to those of the Aged Marine SH category. However, the Convective category exhibited enhanced values of nitrogen species, probably due to emissions from lightning associated with the convection. Values of various species, including peroxides and acids, confirmed that parcels in the category were influenced by the removal of soluble gas and particle species due to precipitation.

Current results were compared with those from the first PEM-Tropics experiment, conducted during August–October 1996. The PEM-T-A period was found to exhibit a much stronger pollution signature than PEM-T-B. PEM-T-A occurred during the southern tropical dry season when there was widespread biomass burning over southern Africa and portions of South America. Conversely, PEM-T-B was conducted during the southern tropical wet season when relatively little biomass burning occurred. Flow patterns during the two periods also exhibited important contrasts. For example, major circulation features were located differently, and the southern hemispheric middle-latitude jet stream was much stronger during PEM-T-A than during PEM-T-B.

In conclusion, current results show that merging trajectory and chemical data is a valuable tool for interpreting the complex chemical signatures that were observed during PEM-T-B. Categorizing the chemical measurements according to their source region also is valuable; however, these categories must be carefully defined so that multiple sources are not combined together.

Acknowledgments. This research was funded by NASA's Tropospheric Chemistry Program. We thank David Westberg for supplying the satellite data used in this research. We appreciate the support of Joe McNeal, Jim Hoell, Jim Raper, and Richard Bendura in helping with the many scientific, logistical, and managerial matters. Similarly, the crews and support staff of the DC-8 and P3-B aircraft always were most helpful during the preparations and deployments of PEM-T-B. We thank Mike Cadena and Erika Harper of the SAIC-GTE Project Office for their assistance during all phases of the project. We appreciate the helpful suggestions of an anonymous reviewer which have improved this paper. Chris Kiley at FSU assisted with the preparation of figures and tables.

References

Andreae, M. O., et al., Methyl halide emissions from savanna fires in southern Africa, *J. Geophys. Res.*, *101*, 23,603–23,613, 1996.

Avery, M. A., D. J. Westberg, H. E. Fuelberg, R. E. Newell, B. E. Anderson, S. A. Vay, G. W. Sachse, and D. R. Blake, Chemical transport across the ITCZ in the central Pacific during an ENSO cold phase event in March/April of 1999, *J. Geophys. Res.*, this issue.

Bhandari, N., D. Lal, and Rama, Stratospheric circulation studies based on natural and artificial radioactive tracer elements, *Tellus*, *18*, 391–405, 1966.

Bieberbach, G., H. E. Fuelberg, A. M. Thompson, A. Schmitt, J. R. Hannan, G. L. Gregory, Y. Kondo, R. D. Knabb, G. W. Sachse, and R. W. Talbot, Mesoscale numerical investigations of air traffic emissions over the North Atlantic during SONEX flight 8: A case study, *J. Geophys. Res.*, *105*, 3807–3820, 2000.

Board, A. S., H. E. Fuelberg, G. L. Gregory, B. G. Heikes, M. G. Schultz, D. R. Blake, J. E. Dibb, S. T. Sandholm, and R. W. Talbot, Chemical characteristics of air from differing source regions during PEM-Tropics A, *J. Geophys. Res.*, *104*, 16,181–16,196, 1999.

Cohan, D. S., M. G. Schultz, and D. J. Jacob, Convective injection and photochemical decay of peroxides in the tropical upper troposphere: Methyl iodide as a tracer of marine convection, *J. Geophys. Res.*, *104*, 5717–5724, 1999.

Danielsen, E. F., Stratospheric-tropospheric exchange based on radioactivity, ozone and potential vorticity, *J. Atmos. Sci.*, *25*, 502–518, 1968.

Davis, D. D., J. Crawford, S. Liu, S. McKeen, A. Bandy, D. Thornton, F. Rowland, and D. Blake, Potential impact of iodine on tropospheric levels of ozone and other critical oxidants, *J. Geophys. Res.*, *101*, 2135–2147, 1996.

Dibb, J. E., R. W. Talbot, K. I. Klemm, G. L. Gregory, H. B. Singh, J. D. Bradshaw, and S. T. Sandholm, Asian influence over the western North Pacific during the fall season: Inferences from lead 210, soluble ionic species, and ozone, *J. Geophys. Res.*, *101*, 1779–1792, 1996.

Dibb, J. E., R. W. Talbot, B. L. Lefer, E. Scheuer, G. L. Gregory, E. V. Browell, J. D. Bradshaw, S. T. Sandholm, and H. B. Singh, Distributions of beryllium-7, lead-210, and soluble aerosol-associated ionic species over the western Pacific: PEM-West B, February–March 1994, *J. Geophys. Res.*, *102*, 28,287–28,302, 1997.

Doty, K. G., and D. J. Perkey, Sensitivity of trajectory calculations to the temporal frequency of wind data, *Mon. Weather Rev.*, *121*, 387–401, 1993.

Ehhalt, D. W., F. Roher, and A. Wahner, Sources and distributions of NO_x in the upper troposphere at northern midlatitudes, *J. Geophys. Res.*, *97*, 9781–9793, 1992.

Elbern, H., J. Kowol, R. Sladkovic, and A. Ebel, Deep stratospheric intrusions: A statistical assessment with model guided analyses, *Atmos. Environ.*, *31*, 3207–3226, 1997.

European Centre for Medium-Range Weather Forecasts (ECMWF), User guide to ECMWF products 2.1, *Meteorol. Bull. M3.2*, Reading, England, 1995.

Fishman, J., K. Fakhruzzaman, B. Cros, and D. Nganga, Identification of widespread pollution in the southern hemisphere deduced from satellite analyses, *Science*, *252*, 1693–1696, 1991.

Fuelberg, H. E., R. O. Loring Jr., M. V. Watson, M. C. Sinha, K. E. Pickering, A. M. Thompson, G. W. Sachse, D. R. Blake, and M. R. Schoeberl, TRACE-A trajectory intercomparison, 2, Isentropic and kinematic methods, *J. Geophys. Res.*, *101*, 23,927–23,939, 1996.

Fuelberg, H. E., R. E. Newell, S. P. Longmore, Y. Zhu, D. J. Westberg, E. V. Browell, D. R. Blake, G. L. Gregory, and G. W. Sachse, A meteorological overview of the Pacific Exploratory Mission (PEM) Tropics period, *J. Geophys. Res.*, *104*, 5585–5622, 1999.

Fuelberg, H. E., J. R. Hannan, P. F. J. van Velthoven, E. V. Browell, G. Bieberbach Jr., R. D. Knabb, G. L. Gregory, K. E. Pickering, and H. B. Selkirk, A meteorological overview of the SONEX period, *J. Geophys. Res.*, *105*, 3633–3651, 2000.

Fuelberg, H. E., R. E. Newell, D. J. Westberg, J. C. Maloney, J. R. Hannan, B. D. Martin, M. A. Avery, and Y. Zhu, A meteorological overview of the second Pacific Exploratory Mission in the Tropics, *J. Geophys. Res.*, this issue.

Garstang, M., P. D. Tyson, R. Swap, M. Edward, P. Kallberg, and A. J. Lindesay, Horizontal and vertical transport of air over southern Africa, *J. Geophys. Res.*, *101*, 23,721–23,736, 1996.

Greenberg, J. P., and P. R. Zimmerman, Nonmethane hydrocarbons in remote tropical, continental, and maritime atmospheres, *J. Geophys. Res.*, *89*, 4764–4778, 1984.

Greenberg, J. P., P. R. Zimmerman, and P. Haagenson, Tropospheric hydrocarbons and CO profiles over the U.S. West Coast and Alaska, *J. Geophys. Res.*, *95*, 14,015–14,026, 1990.

Gregory, G. L., H. E. Fuelberg, S. P. Longmore, B. E. Anderson, J. E. Collins, and D. R. Blake, Chemical characteristics of tropospheric air over the tropical South Atlantic Ocean: Relationship to trajectory history, *J. Geophys. Res.*, *101*, 23,957–23,972, 1996.

Gregory, G. L., et al., Chemical characteristics of Pacific tropospheric air in the region of the Intertropical Convergence Zone and South Pacific Convergence Zone, *J. Geophys. Res.*, *104*, 5677–5696, 1999.

Hannan, J. R., et al., Atmospheric chemical transport based on high-resolution model-derived winds: A case study, *J. Geophys. Res.*, *105*, 3807–3820, 2000.

Harriss, R. C., G. W. Sachse, G. F. Hill, L. Wade, K. E. Bartlett, J. E. Collins, L. F. Steels, and P. C. Novelli, Carbon monoxide and methane in the North American Arctic and subarctic troposphere: July–August 1988, *J. Geophys. Res.*, *97*, 16,589–16,599, 1992.

Heikes, B. G., Formaldehyde and hydroperoxides at Mauna Loa Observatory, *J. Geophys. Res.*, *97*, 18,001–18,013, 1992.

Heikes, B. G., et al., Hydrogen peroxide and methylhydroperoxide distributions related to ozone and odd hydrogen over the North Pacific in the fall of 1991, *J. Geophys. Res.*, *101*, 1891–1905, 1996a.

Heikes, B. G., et al., Ozone, hydroperoxides, oxides of nitrogen, and hydrocarbon budgets in the marine boundary layer over the South Atlantic, *J. Geophys. Res.*, *101*, 24,221–24,234, 1996b.

Hoell, J. M., D. D. Davis, D. J. Jacob, M. O. Rodgers, R. E. Newell, H. E. Fuelberg, R. J. McNeal, J. L. Raper, and R. J. Bendura, Pacific Exploratory Mission in the tropical Pacific A: PEM-Tropics A, August–September 1996, *J. Geophys. Res.*, *104*, 5567–5583, 1999.

Jaeglé, L., et al., Observed OH and H_2O_2 in the upper troposphere suggest a major source from convective injection of peroxides, *Geophys. Res. Lett.*, *24*, 3181–3184, 1997.

Kahl, J. D., A cautionary note on the use of air trajectories in interpreting atmospheric chemistry measurements, *Atmos. Environ., Part A*, *27*, 3037–3038, 1993.

Kawa, S. R., and R. Pearson Jr., Ozone budgets from the dynamics and chemistry of marine stratocumulus experiment, *J. Geophys. Res.*, *94*, 9809–9817, 1989.

Lawrence, M. G., W. L. Chameides, P. S. Kasibhatla, H. Levy II, and W. Moxim, Lightning and atmospheric chemistry: The rate of atmospheric NO production, in *Handbook of Atmospheric Electrodynamics*, edited by H. Volland, pp. 189–202, CRC Press, Boca Raton, Fla., 1995.

LeBel, P. J., W. R. Cofer III, J. S. Levine, S. A. Vay, and P. D. Roberts, Nitric acid and ammonia emissions from a mid-latitude prescribed wetlands fire, *Geophys. Res. Lett.*, *15*, 792–795, 1988.

Lee, M., B. G. Heikes, D. J. Jacob, G. Sachse, and B. Anderson, Hydrogen peroxide, organic hydroperoxide, and formaldehyde as primary products from biomass burning, *J. Geophys. Res.*, *102*, 1301–1309, 1997.

Lee, M., B. G. Heikes, and D. J. Jacob, Enhancements of hydroperoxides and formaldehyde in biomass burning impacted air and their effect on atmospheric oxidant cycles, *J. Geophys. Res.*, *103*, 13,201–13,212, 1998.

Liu, S. C., M. Trainer, F. C. Fehsenfeld, D. D. Parrish, E. J. Williams, D. W. Fahey, G. Hubler, and P. C. Murphy, Ozone production in the rural troposphere and the implications for regional and global ozone distributions, *J. Geophys. Res.*, *92*, 4191–4207, 1987.

Liu, S. C., et al., Model study of tropospheric trace species distributions during PEM-West A, *J. Geophys. Res.*, *101*, 2073–2085, 1996.

McKeen, S. A., and S. C. Liu, Hydrocarbon ratios and photochemical history of air masses, *Geophys. Res. Lett.*, *20*, 2363–2366, 1993.

McKeen, S. A., S. C. Liu, E.-Y. Hsie, X. Lin, J. B. Bradshaw, S. Smyth, G. L. Gregory, and D. R. Blake, Hydrocarbon ratios during PEM-West A: A model perspective, *J. Geophys. Res.*, *101*, 2087–2109, 1996.

Merrill, J. T., R. Bleck, and L. Avila, Modeling atmospheric transport to the Marshall Islands, *J. Geophys. Res.*, *90*, 12,927–12,936, 1985.

O'Sullivan, D., B. G. Heikes, M. Lee, W. Chang, G. L. Gregory, D. R. Blake, and G. W. Sachse, Distribution of hydrogen peroxide and methylhydroperoxide over the Pacific and South Atlantic, *J. Geophys. Res.*, *104*, 5635–5646, 1999.

Pickering, K. E., et al., Convective transport of biomass burning emissions over Brazil during TRACE-A, *J. Geophys. Res.*, *101*, 23,993–24,012, 1996.

Raper, J. L., M. M. Kleb, D. J. Jacob, D. D. Davis, R. E. Newell, H. E. Fuelberg, R. J. Bendura, J. M. Hoell, and R. J. McNeal, Pacific Exploratory Mission in the tropical Pacific: PEM-Tropics B, March–April 1999, *J. Geophys. Res.*, this issue.

Reiter, E. R., M. E. Glasser, and J. D. Mahlman, The role of the tropopause in the stratosphere-troposphere exchange processes, *Pure Appl. Geophys.*, *75*, 185–218, 1969.

Ridley, B. A., et al., Ratios of peroxyacetyl nitrate to active nitrogen observed during aircraft flights over the eastern Pacific Ocean and continental United States, *J. Geophys. Res.*, *95*, 10,179–10,192, 1990.

Shapiro, M. A., Turbulent mixing within tropopause folds as a mechanism for the exchange of chemical constituents between the stratosphere and troposphere, *J. Atmos. Sci.*, *37*, 994–1004, 1980.

Singh, H. B., and P. B. Zimmerman, Atmospheric distribution and sources of nonmethane hydrocarbons, *Adv. Environ. Sci. Technol.*, *24*, 177–235, 1992.

Singh, H. B., et al., Peroxyacetyl nitrate measurements during CITE 2: Atmospheric distribution and precursor relationships, *J. Geophys. Res.*, *95*, 10,163–10,178, 1990.

Smyth, S., et al., Comparison of free tropospheric western Pacific air mass classification schemes for the PEM-West A experiment, *J. Geophys. Res.*, *101*, 1743–1762, 1996.

Stohl, A. G., Computation, accuracy, and applications of trajectories—A review and bibliography, *Atmos. Environ.*, *32*, 947–966, 1998.

Stohl, A., and T. Trickl, A textbook example of long-range transport: Simultaneous observation of ozone maxima of stratospheric and North American origin in the free troposphere over Europe, *J. Geophys. Res.*, *104*, 30,445–30,462, 1999.

Stohl, A., G. Wotawa, P. Seibert, and H. Kromp-Kolb, Interpolation errors in wind fields as a function of spatial and temporal resolution and their impact on different types of kinematic trajectories, *J. Appl. Meteorol.*, *34*, 2149–2165, 1995.

Talbot, R. W., et al., Summertime distribution and relations of reactive odd nitrogen species and NO_y in the troposphere over Canada, *J. Geophys. Res.*, *99*, 1863–1885, 1994.

Talbot, R. W., et al., Chemical characteristics of continental outflow from Asia to the troposphere over the western Pacific Ocean during September–October 1991: Results from PEM-West A, *J. Geophys. Res.*, *101*, 1713–1725, 1996a.

Talbot, R. W., et al., Chemical characteristics of continental outflow over the tropical South Atlantic Ocean from Brazil and Africa, *J. Geophys. Res.*, *101*, 24,187–24,202, 1996b.

Talbot, R. W., et al., Chemical characteristics of continental outflow from Asia to the troposphere over the western Pacific Ocean during February–March 1994: Results from PEM-West B, *J. Geophys. Res.*, *102*, 28,255–28,274, 1997.

van Aardenne, J. A., G. R. Carmichael, H. Levy II, D. Streets, and L. Hordijk, Anthropogenic NO_x emissions in Asia in the period 1990–2020, *Atmos. Environ.*, *33*, 633–646, 1999.

Vincent, D. G., The South Pacific convergence zone: A review, *Mon. Weather Rev.*, *122*, 1949–1970, 1994.

M. A. Avery, J. H. Crawford, and G. W. Sachse, NASA Langley Research Center, Hampton, VA 23681.

D. R. Blake, Department of Chemistry, University of California, Irvine, CA 92717.

H. E. Fuelberg (corresponding author) and J. C. Maloney, Department of Meteorology, Florida State University, Tallahassee, FL 32306-4520. (fuelberg@met.fsu.edu)

B. G. Heikes, Graduate School of Oceanography, University of Rhode Island, Narragansett, RI 02882.

S. T. Sandholm, Department of Earth and Atmospheric Sciences, Georgia Institute of Technology, Atlanta, GA 30332.

H. Singh, NASA Ames Research Center, Moffett Field, CA 94035.

R. W. Talbot, Institute for the Study of Earth, Oceans, and Space, University of New Hampshire, Durham, NH 03824.

(Received September 6, 2000; revised January 31, 2001;
accepted February 19, 2001.)